Chapter 5

Bifurcation analysis of lasers with delay

Bernd Krauskopf
University of Bristol

Lasers, especially semiconductor lasers, are known to exhibit an amazing range of dynamical behaviour when subjected to external influences. In practically all investigations of laser dynamics the question is: how does the dynamics of a given laser system depend on the control parameters?

The approach in a typical experiment is to change one such parameter and record the dynamics, sweeping back and forth to catch possible hysteresis loops. A particular problem for semiconductor lasers is that their dynamics can generally only be recorded in the form of spectra. This is due to the fast time scales in such lasers.

When a mathematical model is available, for example in the form of suitable rate equations, then it is possible to perform numerical simulations. The approach is essentially the same as in an experiment: one or more parameters are changed and the dynamics is recorded. The big advantage is that more information on the solution, and not just its spectrum, is now available, which can be used to interpret and explain the experimental results. Numerical simulation is relatively straightforward, but may be quite expensive in terms of run-time and data storage.

A complimentary approach is that of *bifurcation analysis*. The idea is to find a parameter value where the laser's dynamics changes qualitatively, for example, from stable output to periodic intensity variations. Such a qualitative change is called a *bifurcation*. It is now possible to follow or continue this bifurcation in several parameters with specialised software, called *continuation software*. In this way, one traces out the boundary between two regions of qualitatively different laser dynamics. The collection of bifurcation curves bounding regions of different dynamical behaviour is called a *bifurcation diagram*.

Bifurcation analysis is an established tool that has been used with great success in many fields of application; see Refs. [29, 44, 55, 57] as general references and entry points

to the extensive literature. In laser physics, bifurcation analysis was used with success for laser systems modelled well by ordinary differential equations (ODEs) with low-dimensional phase spaces. A good example is a semiconductor laser with optical injection [65, 67, 68]; this laser system is used throughout the introduction to bifurcation analysis in Ref. [36].

Bifurcation analysis by continuation is not as straightforward as numerical simulation, but it is more powerful. There are two prerequisites for success. First of all, a good knowlegde of bifurcation theory is required, which tells one what bifurcation to expect when one, two, or even more parameters are changed. Secondly, it is necessary to learn how to use continuation software, such as the package AUTO [6] to find and follow bifurcations. Bifurcation analysis is a clear case of 'no pain no gain', or rather, 'some pain a lot to gain'.

It is the goal of this chapter to show how useful bifurcation analysis is when one studies lasers subject to delayed feedback. Examples of such lasers with feedback are a laser receiving *conventional optical feedback* (COF) from an external mirror [16, 47], a laser with *phase-conjugate feedback* (PCF) from an external *phase-conjugating mirror* (PCM) [1, 17, 20, 21, 38, 61]. a laser with opto-electronic feedback [70], and also mutually coupled lasers with delay [33]. While in many applications chaotic laser operation is unwanted, there has been considerable interest in chaotic laser output as a carrier wave form in chaotic communication schemes [15, 62]. In any case, there is a perceived need to study the dynamics and bifurcations of lasers with delay.

These types of laser systems lead to mathematical models that are *delay differential equations* (DDEs). This class of dynamical systems is difficult to study because any DDE has an infinite-dimensional phase space. Section 5.1 introduces what is needed from the mathematical theory of DDEs [5, 31].

An approach not discussed here is to reduce the DDE to a finite-dimensional system. For completeness, here are two examples. Erneux obtains equations for mixed mode solutions in lasers with feedback by multiple time scale analysis; see, for example, [10, 11] and also Sec. 5.3.4. Sieber [56] and Korneyev et al. [35] consider a reduced ODE model obtained by a mode reduction of a traveling wave equation for a multi-section distributed feedback (DFB) laser.

This chapter concentrates entirely on the bifurcation analysis of the *full DDE model*. Until quite recently, the analysis of the linear stability of steady states and direct simulation of the equations were essentially the only tools available to study the dynamics of a given DDEs. This is changing with the development of advanced numerical tools that go well beyond simulation by numerical integration. The Matlab Package DDE-BIFTOOL [9] for the numerical bifurcation analysis of DDEs allows one to follow branches of steady states and periodic solutions in (systems of) DDEs irrespective of their stability. Furthermore, this software is able to detect and continue a number of bifurcations. Using DDE-BIFTOOL to obtain the necessary starting data, it is now also possible to compute special objects in phase space called one-dimensional unstable manifolds [39], which are involved in complicated transitions to chaos. These advanced numerical tools for the bifurcation analysis of DDEs are reviewed in considerable detail in Sec. 5.2.

Lasers with delay have emerged as a major motivation for the development of these new tools, and this chapter reviews some recent results. Section 5.3 presents the bifurcation

analysis of a COF laser as modelled by the Lang-Kobayashi (LK) equations [45]. It reviews results in Ref. [69] on instabilities in lasers with moderate levels of COF and the work in Refs. [30, 49, 50] on connecting bridges of periodic solutions in a semiconductor laser with COF. Section 5.4 reviews recent work in Refs. [24, 25, 26, 28] on the bifurcation analysis of a semiconductor laser with PCF, including a two-parameter bifurcation diagram near the laser's locking range and a sudden transition to chaos via the break-up of a torus.

It must be emphasized that Secs. 5.3 and 5.4 merely constitute a snapshot of the present state-of-the-art, as work on the COF and PCF lasers is ongoing. More generally, the bifurcation analysis of lasers with delay is presently an active and growing field. Examples of research not reviewed here are the work in Refs. [12, 54] on the COF laser with a short external cavity, that in Ref. [53] on a vertical-cavity surface-emitting laser with COF, and that in Ref. [64] on two semiconductor lasers with bidirectional optoelectronic coupling. Other laser systems that can be studied in much the same way are, for example, rate equation models of lasers with opto-electronic or filtered feedback; see also see Chapter 3. More generally, the techniques presented here can also be brought to bear on the bifurcation analysis of DDE models arising in other applications, for example, in control theory [19] and biology [48].

5.1 Bifurcation theory of DDEs

This section is a review of the theory of the basic bifurcations in DDEs with a single fixed delay. (This case is most relevant for laser systems with external feedback. The theory actually holds for any finite number of fixed delays, but becomes more complicated for state-dependent delays; see Ref. [46].) Specifically, the topic of this section is the local bifurcations of equilibria and periodic orbits, and connecting orbits of codimension one. For each respective (local) bifurcation one can find what is known as its *normal form*: a low-dimensional ODE capturing the entire dynamics near the bifurcation in question. This is why bifurcation theory for DDEs with a fixed delay follows that for ODEs.

The exposition in this section is in its nature quite technical and brief; it roughly follows that in Refs. [28, 39]. The emphasis is on the specific situation of a DDE with a single fixed delay, in light of what is needed in later sections. See also Ref. [63] for the basic facts of the theory of DDEs and an application to the LK model, and Refs. [5, 31] for details of the mathematical theory of DDEs.

It is not necessary to work through this section in detail, and the reader is encouraged to jump ahead to the examples and figures of Secs. 5.3 and 5.4. For more background in general bifurcation theory see the introductory text Ref. [36], or a text book with examples from laser physics such as Ref. [57].

The bifurcations of codimension one treated here are not only the most important ones that one expects to find in any DDE, but also those that can now be found and followed with the continuation package DDE-BIFTOOL [9], as is explained in Sec. 5.2.2.

5.1.1 The phase space of a DDE

A DDE with a single fixed delay $\tau \in \mathbb{R}$ is of the general form

$$\frac{dx(t)}{dt} = F(x(t), x(t-\tau), \eta)\,. \tag{5.1}$$

The variable x is from the *physical space*, which is taken to be $\mathbb{R}^n$, and $\eta \in \mathbb{R}^p$ is a multi-parameter. (For the laser systems discussed later the physical space is three-dimensional (E, N)-space, where E is the complex electric field and N is the inversion.) The function

$$F : \mathbb{R}^n \times \mathbb{R}^n \times \mathbb{R}^p \to \mathbb{R}^n$$

describing the right-hand side of Eq. (5.1) is differentiable.

It is important not to confuse the physical space of Eq. (5.1) with its *phase space*, which is the infinite-dimensional space of continuous functions $\mathcal{C}$ over the delay interval $[-\tau, 0]$ with values in $\mathbb{R}^n$. In physical terms, this means that one needs to prescribe an entire history of length τ in order to determine the future evolution of the system described by Eq. (5.1). In other words, unlike for ODEs, prescribing a single initial condition in the physical space $\mathbb{R}^n$ is not enough.

As is usual in any phase space, one speaks of a *point* $q \in \mathcal{C}$ in phase space, which is a continuous function

$$q : [-\tau, 0] \to \mathbb{R}^n$$

over the delay interval with values in physical space. The point $q(0)$ is called the *head* of q and $\{q(t) \mid t \in [-\tau, 0)\}$ its *history*. The future of every point q in the phase space $\mathcal{C}$ after time t is uniquely determined by Eq. (5.1) for any positive $t \in \mathbb{R}$. This gives rise to the *evolution operator*

$$\Phi^t : \mathcal{C} \to \mathcal{C}$$

which prescribes how an initial point $q \in \mathcal{C}$ evolves after time t. This is sketched in Fig. 5.1 in projection onto the physical space $\mathbb{R}^n$, where the point q can be thought of as moving along its trajectory much like a train over a roller coaster track. The *solution* starting from q is then given as

$$x : [0, \infty) \to \mathbb{R}^n\,, \quad t \mapsto \Phi^t(q)\,.$$

5.1.2 Local bifurcations of steady states

A *steady state* of Eq. (5.1) is a point q_0 such that $q_0(t) \equiv x_0$ for all $t \in [-\tau, 0]$ and some fixed $x_0 \in \mathbb{R}^n$. In other words, $F(q_0, q_0, \eta^*) = 0$ (for some fixed value η^* of the parameter η) and $\Phi^t(q_0) = q_0$ for all $t > 0$. Again, it is important not to confuse the fixed value x_0 in physical space with the constant function q_0 over the delay interval, which is a point in phase space. The stability of q_0 is given by the linearization of Eq. (5.1) around q_0 (acting on a point $q \in \mathcal{C}$)

$$DF(q_0, \eta^*)\, q = A_1(q_0, \eta^*) q(t) + A_2(q_0, \eta^*) q(t-\tau)\,. \tag{5.2}$$

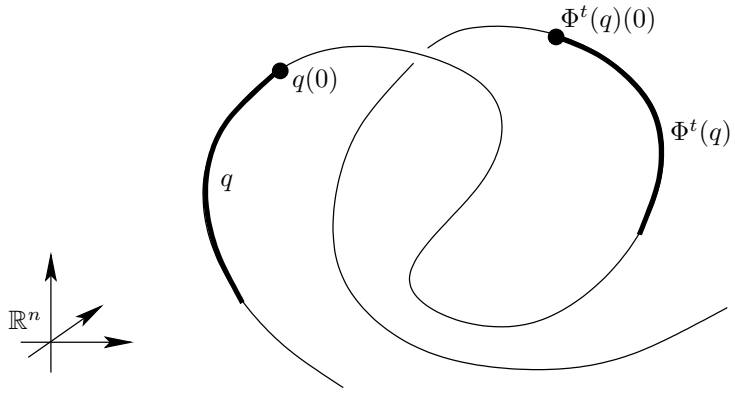

Figure 5.1: The evolution operator Φ^t of a DDE acting on a point $q \in \mathcal{C}$, shown in projection onto the physical space $\mathbb{R}^n$.

The linearization is the generalization of the Jacobian of an ODE to the setting of DDEs. The matrices A_1 and A_2 are given as

$$A_1(q_0, \eta^*) := \left.\frac{\partial F(u, v, \eta)}{\partial u}\right|_{(x_0, x_0, \eta^*)} \text{ and } \quad A_2(q_0, \eta^*) := \left.\frac{\partial F(u, v, \eta)}{\partial v}\right|_{(x_0, x_0, \eta^*)} \tag{5.3}$$

where $u, v \in \mathbb{R}^n$ were used as the arguments of $F(u, v, \eta)$.

The stability of Eq. (5.1) near q_0 can be found by considering the eigenvalues of the $n \times n$ matrix

$$\Delta(q_0, \eta^*, \lambda) := \lambda I - A_1(q_0, \eta^*) - A_2(q_0, \eta^*) e^{-\lambda\tau}\,, \tag{5.4}$$

which are given as the roots of the *characteristic equation*

$$\det(\Delta(q_0, \eta^*, \lambda)) = 0\,. \tag{5.5}$$

Due to the transcendental nature of Eq. (5.5) there are infinitely many eigenvalues. This makes the study of DDEs much harder than that of ODEs.

However, a DDE with a fixed delay has the crucial property that the eigenvalues of Eq. (5.4) are discrete. This means that there are no accumulation points of eigenvalues in the complex plane, and that there is no essential spectrum (a continuous part of the spectrum). What is more, for any fixed $\gamma > 0$ there are always finitely many eigenvalues with real part larger than γ. For the special case that $\gamma = 0$ one gets the result that there are always only finitely many unstable eigendirections (associated with eigenvalues with real part greater than zero); for further details see Ref. [5].

A steady state is called *hyperbolic* if there are no eigenvalues that have zero real part. A hyperbolic steady state is either attracting or a saddle point, the latter having infinitely many attracting and finitely many repelling eigendirections.

When the parameter η is changed, eigenvalues can cross the imaginary axis of the complex plane, leading to changes in the stability of the equilibrium. Because the eigenvalues are isolated, when a single parameter is changed there are only two generic or typical possibilities (for a DDE without any extra symmetry properties), giving rise to the two local bifurcations of steady states of codimension one:

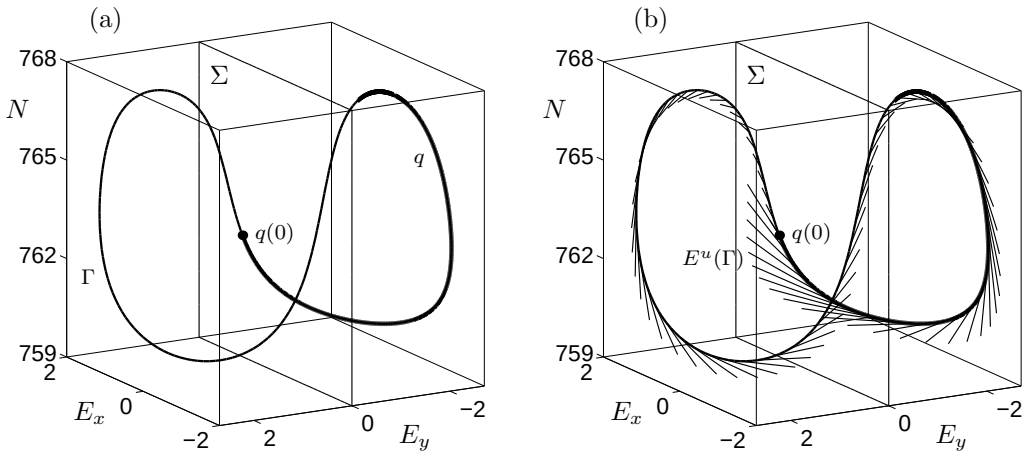

Figure 5.2: A periodic orbit Γ of the DDE and a fixed point q (boldface) of a suitable Poincaré map P (a), and the linear unstable eigenspace $E^u(\Gamma)$ (b) in the projection onto physical space; the example is of Eqs. (5.23) and (5.24) for $I = 65.1\,\mathrm{mA}$ and $\kappa\tau = 1.9266$.

1. A single real eigenvalue goes through zero. This is the case of a *saddle-node bifurcation* in which two equilibria are born.

2. A complex conjugate pair of eigenvalues move across the imaginary axis of the complex plane. This is the case of a *Hopf bifurcation* from which a small periodic orbit bifurcates.

In order to check that one is dealing with either of these bifurcations one has to check the so-called genericity conditions, which is difficult in practice as it involves computing the normal form on a center manifold. However, the good news is that these conditions are typically satisfied. If they are not satisfied then one is dealing with degeneracy, such as a bifurcation of higher codimension.

The Hopf bifurcation may be supercritical or subcritical, depending on whether the bifurcating periodic orbit is attracting or not. This is easy enough to detect in practice, so that tedious computations involving third-order terms can generally be avoided.

5.1.3 Local bifurcations of periodic orbits

A *periodic orbit* is a solution Γ such that $\Phi^{\mathsf{T}}(q) = q$ for some period $\mathsf{T} > 0$ and all $q \in \Gamma$. In projection onto the physical space $\mathbb{R}^n$, the periodic orbit Γ is a closed curve. As for ODEs, the Poincaré map P is defined as the return to a suitable section Σ transverse to Γ. In what follows a section $\Sigma \subset \mathbb{R}^n$ is fixed and $\mathcal{C}_\Sigma$ denotes the space of points in $\mathcal{C}$ with headpoints in Σ. The Poincaré map P is defined as

$$P:\ \mathcal{C}_\Sigma \to \mathcal{C}_\Sigma, \quad q \mapsto \Phi^{t_q}(q)\,, \tag{5.6}$$

where $t_q > 0$ is the return time to Σ. Note that it is always possible to find a section Σ (locally) transverse to a periodic orbit Γ, and a Poincaré map P so that $q \in \Gamma$ with $q(0) \in \Sigma$ is a fixed point under P. (Note that $\Phi^{\mathsf{T}}(q) = q$.) This is illustrated in Fig. 5.2 (a).

The stability of the periodic orbit Γ is given by its Floquet multipliers. They can be found as the eigenvalues of the linearization $DP(q)$ of the Poincaré map P around the associated fixed point $q \in \mathcal{C}_\Sigma$. (Note that there is always the extra trivial Floquet multiplier at $+1$, corresponding to the eigendirection along Γ.) To find $DP(q)$ one needs to compute the linear variational equation around Γ, which, in general, has T-periodic coefficients [5].

The linearization $DP(q)$ has a spectrum that consists of countably many eigenvalues (the Floquet multipliers). It has the origin of the complex plane as its only accumulation point. In other words, much like in the situation for equilibria, there are only a finite number of Floquet multipliers outside a circle of fixed radius $r > 0$. For the special case of $r = 1$ one gets the result that there are always only a finite number of unstable Floquet multipliers.

A periodic orbit Γ is called hyperbolic if there are no Floquet multipliers on the unit circle (except for the trivial one). A hyperbolic periodic orbit is either attracting if all the Floquet multipliers are inside the unit circle or of saddle type with infinitely many attracting and finitely many repelling eigendirections.

When the parameter η is changed, Floquet muiltipliers can cross the unit circle of the complex plane, leading to changes in the stability of the periodic orbit Γ. Because the Floquet muiltipliers are isolated (away from the origin of the complex plane), when a single parameter is changed there are exactly three generic or typical possibilities (for a DDE without any extra symmetry properties), giving rise to the local bifurcations of periodic orbits of codimension one:

1. A single real Floquet multiplier goes through $+1$. This is the case of a *saddle-node bifurcation of limit cycles* in which two periodic orbits are born.

2. A single real Floquet multiplier goes through -1. This is the case of a *period-doubling bifurcation* in which a new periodic orbit of period $2\mathsf{T}$ bifurcates.

3. A complex conjugate pair of Floquet multipliers moves through the unit circle of the complex plane at $e^{2\pi i\alpha}$. Provided that $\alpha \neq 0, \frac{1}{2}, \frac{1}{3}, \frac{2}{3}, \frac{1}{4}, \frac{3}{4}$ then this is the case of a *torus (or Neimark-Sacker) bifurcation*, in which an invariant torus is born. (The conditions on α are to avoid the more complicated strong resonances; see, for example, Refs. [37, 44] for details.)

In order to check that one is dealing with any of these bifurcations one has to check the respective genericity conditions. Again, these conditions are typically satisfied, which is good because it is even harder to verify them for periodic orbits. The reason for this is that the Poincaré map P and its linearization cannot be computed explicitly, but must be computed numerically.

The period-doubling bifurcation and the torus bifurcation may be supercritical or subcritical, depending on whether the bifurcating object is attracting or of saddle type. This is usually apparent from the bifurcation scenario being considered, so that it is generally not necessary to compute the respective normal form coefficients, which involve higher-order terms.

5.1.4 Unstable manifolds and global bifurcations

Associated with a saddle steady state q_0, there are a finite number of unstable eigenfunctions of the linearization around q_0, which span the linear unstable eigenspace $E^u(q_0)$. The *local unstable manifold* $W^u_{\rm loc}(q_0)$ is the set of points q that can be integrated backwards, never leave a small neighbourhood V of q_0 under Φ^t for $t < 0$, and are such that $\Phi^t(q) \to q_0$ as $t \to -\infty$. As is the case for ODEs, $W^u_{\rm loc}(q_0)$ is tangent to $E^u(q_0)$ at q_0 and of the same dimension (given by the number of unstable eigenvalues). The (global) unstable manifold $W^u(q_0)$ is defined as the globalization of $W^u_{\rm loc}(q_0)$:

$$W^u(q_0) = \{\Phi^t(p) \mid p \in W^u_{\rm loc}(q_0) \text{ and } t > 0\}\,.$$

The *stable manifold* $W^s(q_0)$ is defined similarly as the set of points that converge to q_0 under Φ^t in positive time, but it is always infinite-dimensional since there are infinitely many stable eigenvalues of the linearization around q_0.

An important special case is that of a one-dimensional unstable manifold $W^u(q_0)$, because then $W^u(q_0)$ is a smooth 1D curve in projection onto the physical space $\mathbb{R}^n$. In particular, the manifold $W^u(q_0)$ has two branches, one on either side of $W^s(q_0)$, which can be computed efficiently by integrating from two initial conditions near q_0 on $E^u(q_0)$. If $W^u(q_0)$ lies in $W^s(q_0)$ then it forms a *codimension-one homoclinic connection*. If $W^u(q_0)$ lies in $W^s(q_1)$ for a different saddle point $q_1 \in \mathcal{C}$ with a one-dimensional unstable manifold then it forms a *codimension-one heteroclinic connection* between q_0 and q_1. At the connection, which occurs for some fixed value η^* of the parameter η, there is a solution $x(t)$ of Eq. (5.1) such that the limits

$$\lim_{t\to-\infty} x(t) = q_0, \qquad \lim_{t\to+\infty} x(t) = q_{0,1}, \tag{5.7}$$

exist. Homoclinic and heteroclinic connections are important for the overall organization of phase space. As is explained in Sec. 5.2.2, they can be found and followed by continuation [52].

A periodic orbit Γ of saddle-type comes with unstable manifolds as well. In what follows, the case is considered that Γ has a single unstable Floquet multiplier, where there is a single unstable eigenfunction spanning the linear unstable eigenspace $E^u(\Gamma)$. In projection onto physical space $E^u(\Gamma)$ forms a one-parameter family of directions along Γ. This is illustrated in Fig. 5.2 (b).

Again, consider the associated saddle fixed point $q \in \mathcal{C}_\Sigma$ of a suitable Poincaré map P to a section Σ and define the *local unstable manifold* $W^u_{\rm loc}(q)$ of q as the set of all points $p \in \mathcal{C}_\Sigma$ that can be iterated backwards under P, never leave a small neighbourhood V of q, and are such that $P^l(p) \to q$ as $l \to -\infty$. The manifold $W^u_{\rm loc}(q)$ is tangent to $E^u(q)$ (which can be derived from $E^u(\Gamma)$) and of the same dimension, in our case dimension one. The (global) unstable manifold $W^u(q)$ is the globalization of $W^u_{\rm loc}(q)$ defined by

$$W^u(q) = \{P^l(p) \mid p \in W^u_{\rm loc}(q) \text{ and } l > 0\}\,.$$

The stable manifold $W^s(q)$ is defined similarly as the set of points that converge to q under P in positive time, and it is always infinite-dimensional [31].

In projection onto the physical space $\mathbb{R}^n$ the unstable manifold $W^u(q)$ forms a complicated two-dimensional object. However, the set of its headpoints in Σ, which is called its *trace*, is a 1D curve that is smooth (except possibly at isolated points due to the projection), very much like the 1D unstable manifold of a saddle point of a finite-dimensional map. The difference in the case of DDEs is that the trace $W^u(q) \cap \Sigma$ may have self-intersections, which is a clear reminder of the fact that $W^u(q)$ lives in an infinite-dimensional phase space.

As for ODEs, the study of 1D unstable manifolds of saddle points of the Poincaré map is a powerful tool when one wants to study transitions to chaos. With the method explained in Sec. 5.2.3 they can now be computed; this is demonstrated in Sec. 5.4.4 with the example of the break-up of an invariant torus in the PCF laser [26].

5.2 Numerical methods

This is an exciting time to study lasers with delay. Powerful new numerical techniques are now becoming available, similar to those that have been used for many years and with great success for the study of finite-dimensional dynamical systems defined by ODEs. Most importantly, the continuation package DDE-BIFTOOL [9] allows one to find and follow steady states and periodic orbits irrespective of their stability, a great advantage over mere simulation which only finds stable objects. DDE-BIFTOOL can detect and follow codimension-one bifurcations. This package is still under development and lasers with feedback have emerged as arguably the most important motivation and application for recent additions to its capabilities [26, 28]. Building on the computation of saddle periodic orbits to obtain the necessary starting data, a method for computing 1D unstable manifolds was developed in Ref. [39].

These numerical methods are now reviewed in quite some technical detail, because they are still not widely known in the field of laser physics. The reader is again invited to look ahead at Secs. 5.3 and 5.4 to see how they can be used to analyze the dynamics of lasers with delay.

5.2.1 Simulation by direct numerical integration

The most basic operation is to integrate a DDE to simulate the dynamics. After transients have died away, the dynamics will settle down to some attractor of the DDE. (Here it is assumed that the DDE is dissipative, as is the case for laser systems). A DDE with a fixed delay is best integrated with a fixed time-step method, where the time step is chosen as an integer fraction τ/M of the delay time τ. This means that the history interval $[-\tau, 0]$ is discretised into M equal subintervals. A single integration step then produces a numerical approximation of the evolution operator $\Phi^{\tau/M}$ over the time step τ/M. As was explained in Sec. 5.1.1, one needs to initialize and keep the entire (discretization of the) history array during a computation.

In the simplest case one could use forward Euler integration. Other more involved and efficient integration routines, such as Runge-Kutta integrators, require storing a few more elements in the history array as input to the integrator. In the simulations in Sec. 5.4 an

Adams-Bashforth fourth-order multistep method was used. This requires storing a list up to and including the vector $q(-\tau - 3\frac{\tau}{M})$, that is, three extra elements.

Numerical simulation has been used for many years to study the dynamics of lasers with delay. Typically, one real variable, for example, the inversion at a given value of the electric field, is plotted after transients died down for a range of a control parameter. In this way, one gets a one-parameter bifurcation plot of how the attractor in the system changes with the parameter. This approach can be found virtually everywhere, for examples, in Refs. [16, 21, 38, 47], in Chapters 3 and 4, and in Figs. 5.10 (a) and 5.15 (a). It provides a good way of getting an impression of the attracting dynamics of the laser.

5.2.2 Numerical continuation

The idea of numerical continuation is to find an object of interest and then follow it in suitable parameters. The big advantage is that this object can be followed irrespective of its stability. This means that information can be obtained also about objects that are not attracting, which is a big advantage over numerical simulation.

Mathematically, continuation is set up in such a way that there are $L-1$ equations for L unknown variables, so that the solution space is geometrically a one-dimensional curve in $\mathbb{R}^L$. Once a first point on this solution curve is found, then it is possible to follow or continue it in the parameters. This is usually done with the method called pseudo-arclength continuation, which involves a prediction step in the direction tangent to the curve and a Newton correction step in the space perpendicular to this tangent. During a computation the stepsize along the branch is adapted in response to the success of the Newton correction.

The idea of continuation can be used to follow branches of many implicitly defined problems, including bifurcations. It is implemented, for example, in the much used continuation package AUTO [6] for (among other things) the bifurcation analysis of ODEs. It must be stressed that the technique of numerically solving appropriately formulated bifurcation equations by continuation is firmly established (with proofs of convergence) in the field of numerical analysis. Admittedly, using numerical continuation requires the user to know a good deal more about bifurcation theory than is needed for numerical simulation. The reward is a very powerful tool that, if used properly (that is, with some experience and the necessary checks), allows one to unravel even complicated dynamics in great detail and with great accuracy. See, for example, Ref. [55] for more general background reading in the context of ODEs.

Here we concentrate on the numerical continuation in DDEs. The recently developed continuation package DDE-BIFTOOL [9] consists of Matlab routines for the continuation and bifurcation analysis of steady states and periodic solutions. DDE-BIFTOOL solves a large system that is obtained by discretizing the delay interval $[-\tau, 0]$ and uses pseudo-arclength continuation to follow solution branches. This package detects and follows saddle-node and Hopf bifurcations of steady states, and detects the local codimension-one bifurcations of periodic orbits, namely saddle-node bifurcations of limit cycles, period-doubling bifurcations and torus bifurcations. (The continuation of bifurcations of periodic orbits is not yet implemented.)

A steady state is represented by the value of the parameter η, the steady state position

x_0 and the eigenvalues λ_i of this steady state. These eigenvalues λ_i are found as the (appropriate number) of right-most roots of the characteristic equation Eq. (5.4), which are corrected using Newton iterations. A saddle-node bifurcation is detected and represented by a null-vector of the matrix $\Delta(0)$ in Eq. (5.4), and a Hopf bifurcation by the complex null vector of $\Delta(i\omega)$ for a corresponding frequency ω.

Periodic solutions are represented by a suitable boundary value problem, which is solved by orthogonal collocation, which is a piecewise polynomial representation of the solution. Specifically, a periodic solution is represented by the value of the parameter η, the period T and a profile $x^*(t/\mathsf{T})$ on a mesh over the (time-scaled) interval $[0, 1]$. The stability information for periodic orbits is obtained by computing a finite number of the largest Floquet multipliers (for example, all those outside a suitable radius $r > 0$).

The software package DDE-BIFTOOL is able to switch to and continue emanating branches of periodic orbits at bifurcation points (such as a Hopf bifurcation), and continue codimension-one bifurcations of steady states in two parameters. DDE-BIFTOOL can be extended to monitor other test functions that might be of interest to users. An example is the detection and continuation of a neutral saddle-focus point in Ref. [28].

A recent addition to DDE-BIFTOOL is the computation of connecting orbits and their continuation in two parameters [52]. This algorithm uses what are known as projection boundary conditions (appropriately adapted to the context of DDEs) and is a natural extension of the method that was implemented for the computation of connecting orbits of ODEs in the HomCont [3] extension of AUTO. The computation of a connecting orbit can be started from a nearby periodic orbit with a sufficiently large period.

As will be illustrated with the examples in Secs. 5.3 and 5.4, the usefulness of DDE-BIFTOOL for the bifurcation study of lasers with delay, and of DDEs in general, can hardly be exaggerated. For more details on the inner workings of DDE-BIFTOOL see Refs. [7, 8, 9, 52].

5.2.3 Computation of 1D unstable manifolds

Suppose that q_0 is a steady state with one unstable eigenvalue, that is, with a one-dimensional linear unstable eigenspace $E^u(q_0)$. As was explained in the previous section, q_0 can be found by numerical continuation. The unstable eigenspace is spanned by a (generalized) vector $v : [-\tau, 0] \to \mathbb{R}^n$ of linear directions along q_0. This vector v can be found by an iterative approach or directly with DDE-BIFTOOL; see Refs. [26, 39]. Both branches of the 1D unstable manifold $W^u(q_0)$ can then be computed by integrating from the initial conditions $q_0 \pm \delta v$ for a suitably small $\delta > 0$, that is, from initial conditions on $E^u(q_0)$ close to q_0.

It is much more challenging to compute the 1D unstable manifold of a saddle fixed point $q \in \mathcal{C}_\Sigma$ of a Poincaré map (associated with a saddle periodic orbit Γ). The 1D linear unstable eigenspace $E^u(\Gamma)$ can again be found as a vector v by an iterative approach. The computation of v using DDE-BIFTOOL has recently been developed [27]. This allows us to find as starting data a first point $q \pm \delta v \in \mathcal{C}_\Sigma$ at a small distance δ from q along $E^u(\Gamma)$ (whose headpoint lies in Σ); see Fig. 5.2 (b).

The idea is now to 'grow' a branch of $W^u(q)$ step by step until a sufficiently long piece has been computed. In fact, any of the known algorithms for computing 1D un-

stable manifolds of saddle points of finite-dimensional maps can be generalized to the setting of DDEs by working on points in $\mathcal{C}_\Sigma$, instead of on points in a finite-dimensional space. However, points in $\mathcal{C}_\Sigma$ are computationally expensive to work with because they are represented by $(M \times n)$ data arrays (where n is the dimension of the physical space $\mathbb{R}^n$). It is therefore imperative to compute as few points as necessary to achieve a prescribed accuracy of the computation. For this reason the generalization of the growth method in Refs. [41, 42] was implemented. All relevant operations, such as the iteration of the Poincaré map and interpolation, were interpreted and implemented as operations on points in $\mathcal{C}_\Sigma$, or rather on their discretizations as data arrays.

A sketch of the algorithm is presented here for completeness; see Ref. [39] for a detailed explanation. A branch of the 1D unstable manifold $W^u(q)$ is represented by a list $\{p_1, p_2, \ldots, p_k\}$ of points in $\mathcal{C}_\Sigma$. Linear interpolation is used between consecutive list points. The algorithm proceeds in steps by computing one new point at a time, hence, growing the list representing the branch. To find the next point p_{k+1} in the list one searches for a point in the part of $W^u(q)$ that was already computed (this requires interpolation between mesh points) that maps to a circle of a predetermined radius Δ_k around the last point p_k. Because of the invariance of $W^u(q)$, this new point p_{k+1} lies on $W^u(q)$ in good approximation. The distance Δ_k is adapted during the computation depending on the curvature of the trace of the manifold $W^u(q) \cap \Sigma$ in the section Σ. A computation stops after a prescribed arclength distance of the trace $W^u(q) \cap \Sigma$ has been reached or when convergence to an attracting fixed point is detected.

The only way of checking the accuracy of a computation in practice is to compare the results of successive computations with increased accuracy. (It is impossible to derive *a priori* bounds of any global manifold computation. To test the algorithm, it was also compared with the method of fundamental domain iteration, which does not involve interpolation, an important contributor to the overall error; see Ref. [39].) The method works reliably, provided that sufficiently small error bounds are chosen. Clearly, the longer and more complicated the manifold becomes, the more careful one has to be. The examples in Sec. 5.4.4 show that the method can be used successfully to study global bifurcations in a laser with delay.

5.3 Bifurcations in the COF laser

A semiconductor laser receiving optical feedback from a mirror placed at a fixed distance L is the classic example of a laser subject to delay. One also speaks of a laser with conventional optical feedback (COF) or an external cavity laser. This laser system is physically straightforward, technologically relevant and has received a lot of attention, both experimentally and in terms of mathematical modelling. There is an extensive body of literature on the subject; see, for example, the recent surveys Refs. [14, 16, 59, 60] and Chapters 1, 2 and 4 for more background material and further references.

There is a well-established rate equation model of the COF laser, the so-called Lang-Kobayashi (LK) equations [45]. They can be written in the dimensionless form

$$\frac{dE}{dt} = (1+i\alpha)N(t)E(t) + \kappa e^{-iC_p}E(t-\tau) \tag{5.8}$$

$$T\frac{dN}{dt} = P - N(t) - (1+2N(t))|E(t)|^2 \tag{5.9}$$

for the complex electric field $E = E_x + iE_y$ and the inversion N. The parameters are the pump current P, the ratio of decay times T, the linewidth-enhancement factor α, the feedback strength κ, the delay time $\tau = 2L/c$ (where c is the speed of light), and the feedback phase C_p. In fact, $C_p = \omega_0\tau$, where ω_0 is the optical frequency. However, C_p is generally seen as an independent parameter because it can be changed by miniscule changes of, for example, the length of the external cavity (using a PZT) or the pump current [32, 34].

The LK equations are based on two main modelling assumptions, namely that the laser operates in single mode and that the feedback is not too strong. This allows Eqs. (5.8) and (5.9) to describe only one mode and to take into account a single round-trip in the external cavity. Implicitly, this also means that the external cavity length L should be larger than the length of the laser itself; in most experiments it is of the order of centimeters to meters. While one should be aware of the underlying modelling assumptions, the LK equations are known to describe many experimentally observed dynamics with amazing accuracy; see again Chapter 4 for more examples.

Complicated dynamics in the LK equations have been studied mainly by direct numerical simulation. However, when advanced numerical methods for DDEs recently became available, the LK equations emerged as a natural first application. The following sections review some recent work on the bifurcation analysis of the COF laser as modelled by the LK equations.

5.3.1 Symmetry of the COF laser equation

The LK equations are a DDE of the form Eq. (5.1) and their physical space is the three-dimensional (E, N)-space. So it seems that one can immediately apply the tools of bifurcation theory introduced in Sec. 5.2 to Eqs. (5.8) and (5.9). However, this is not the case, because the LK equations feature an important symmetry: they are invariant under the continuous symmetry group S^1 of all rotations of the complex E-plane. This symmetry group can be written as $S^1 = \{c \in \mathbb{C} \mid |c| = 1\}$ and an element $c \in S^1$ acts on a trajectory

$(E, N)(t)$ of Eqs. (5.8) and (5.9) by

$$c \circ (E, N)(t) = (cE, N)(t)\,. \tag{5.10}$$

This means that the rotation over of any angle $\phi = \arg(c)$ of a trajectory is again a trajectory! In other words, a trajectory is either S^1-symmetric itself, or it is not isolated but comes as a rotational family parametrized by the elements of S^1.

This S^1-symmetry is not an artefact of the LK equations, but is also present in other rate equation models of COF lasers; see Ref. [43] for details. It is a consequence of two properties: Eq. (5.8) is linear in E, and E enters Eq. (5.9) only as its modulus $|E|$. The continuous symmetry group S^1 of the LK equations cannot be divided out. However, as is explained below, bifurcation techniques can still be brought to bear on the system after appropriate modifications.

Let us start with some thoughts about the physical space. If one writes E in polar coordinates as $E(t) = R(t)e^{i\varphi(t)}$ then the action of $c \in S^1$ on E is that of adding $\arg(c)$ to $\varphi(t)$. It is sufficient to consider the intersection (also called the trace) of all S^1-images of a trajectory $(E, N)(t)$ with the two-dimensional half-plane $\{(E, N)\,|E_y = 0 \text{ and } E_x \geq 0\}$. This half plane can simply be identified with the (R, N)-plane, which emerges as a *reduced physical space*. In practice, to obtain the trace all one needs to do is plot N versus R. This is only a useful projection; the φ-dynamics is important and cannot be neglected.

5.3.2 External cavity modes

The most basic solution of Eqs. (5.8) and (5.9) is the trivial solution $(E, N)(t) \equiv (0, P)$ (where P is the pump current). If it is stable then the laser is in its off-state. The laser threshold is given by the loss of stability of the trivial solution. In Eqs. (5.8) and (5.9) this occurs in a Hopf bifurcation. (When the electric field equation (5.8) is written in polar coordiantes the threshold is given by a pitchfork bifurcation, and when Eq. (5.8) is written in terms of the power $|E|^2$ it is given by a transcritical bifurcation.) In the Hopf bifurcation a small periodic orbit is born. The laser does produce constant output, as is expected just above threshold (when this periodic orbit is stable), because it turns out that this periodic orbit is of a special form with constant R and N. Indeed it is one of the external cavity modes that are introduced now.

An *external cavity mode* (ECM), also referred to as a continuous wave solution or CW-state, is a solution of Eqs. (5.8) and (5.9) of the form

$$(E, N)(t) = (R_s e^{i\omega_s t}, N_s) \tag{5.11}$$

for constant R_s, ω_s and N_s. In other words, an ECM is a perfectly circular periodic orbit in (E, N)-space of period $2\pi/\omega_s$. In projection onto the (R, N)-plane an ECM is a single point; in some papers ECMs are referred to as fixed points.

By writing Eqs. (5.8) and (5.9) in polar coordinates and inserting (5.11) as an ansatz, one obtains

$$R_s^2 = \frac{P - N_s}{1 + 2N_s} \tag{5.12}$$

$$\omega_s = -\kappa(\alpha \cos(\omega_s \tau + C_p) + \sin(\omega_s \tau + C_p)) \tag{5.13}$$

$$N_s = -\kappa \cos(\omega_s \tau + C_p) \tag{5.14}$$

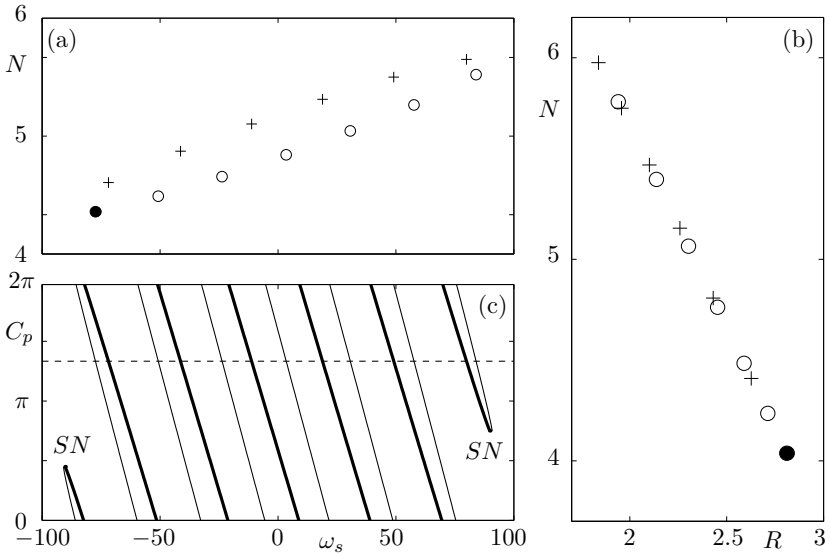

Figure 5.3: An ellipse of ECMs (a) in the (ω_s, N)-plane and the same ECMs in the (R, N)-plane (b); modes are circles and anti-modes crosses, the black dot is a stable ECM, also called the maximum gain mode. The ECMs can be continued as one branch in the 2π-periodic parameter C_p (c); the ECMs in (a) and (b) correspond to the value of $C_p = \frac{3}{4}\pi$ indicated by the dashed line in (c). The LK equations and the other parameters are as in Ref. [34].

where it is assumed that $R_s \neq 0$ (and $N_s \neq -\frac{1}{2}$). These equations have the structure, that once ω_s is known, N_s and then R_s can be found. However, Eq. (5.13) is transcendental and cannot be solved explicitly. It can be rewritten as

$$\omega_s = -\frac{K}{\tau}\sin(\omega_s\tau + C_p + \arctan(\alpha)) \tag{5.15}$$

where $K = \kappa\tau\sqrt{\alpha^2+1}$ (also called the effective feedback strength). In other words, the solutions of Eq. (5.15) are the intersection of a sine function with amplitude $\frac{K}{\tau}$ with the diagonal (the graph of the function $f(w_s) = w_s$). This already shows that there is always at least one solution of Eq. (5.13). When κ is increased more solutions are created in pairs, which already shows that new ECMs are born in saddle-node bifurcations. In particular, one ECM (the one with lower N_s) of a newly-born pair is initially attracting, while the other is a saddle. Furthermore, as is expected already from Eqs. (5.8) and (5.9), the solution set of Eq. (5.15) is 2π-periodic in the feedback phase C_p.

It is important to realize that, in order for a solution of Eqs. (5.12)–(5.14) to be physically relevant, the radius R_s must be positive. Since the pump current P is positive, this implies that

$$-\frac{1}{2} < N_s \leq P\,. \tag{5.16}$$

It is well-known that the ECMs lie on an ellipse in a suitable projection, for example in the (ω_s, N)-plane as is shown in Fig. 5.3 (a). In projection onto the (R, N)-plane all

ECMs lie on a straight line; see Fig. 5.3 (b). The ECMs on the lower part of the elllipse (that are initially stable) are often referred to as modes, and those on the upper part as anti-modes. The ellipse is entirely in the physically relevant region if condition (5.16) is satisfied. Otherwise, only part of it corresponds to physical ECMs. By changing C_p over several cycles of 2π, an individual ECM can be followed from its emergence in a saddle-node bifurcation to its disappearance in another saddle-node bifurcation. This is shown in Fig. 5.3 (c) in the (ω_s, C_p)-plane; the ellipse in Fig. 5.3 (a) for a fixed value of $C_p = \frac{3}{4}\pi$ corresponds to a cross section through this image.

These results on the ECMs are now classical; see Chapter 2. The solutions of Eqs. (5.12)–(5.14) can be found, for example, by Newton's method. However, the following sections stress the point of view of bifurcation theory. Indeed Eqs. (5.12)–(5.14) are implicit equations whose solutions, the ECMs, can best be computed by starting at a first ECM and then continuing it in parameters.

5.3.3 The characteristic equation of an ECM

The next step is to consider and compute the stability of the ECMs in order to find and continue their bifurcations. To do this one needs to compute the linear variational equation around an ECM, because the ECMs are after all periodic orbits, not steady states. Following the procedure in Ref. [63] and writing Eqs. (5.8) and (5.9) in polar coordinates, they take the form

$$\frac{d}{dt}\begin{pmatrix} R(t) \\ \phi(t) \\ N(t) \end{pmatrix} = F(R(t), \phi(t), N(t), R(t-\tau), \phi(t-\tau))\,. \tag{5.17}$$

The function F is defined as

$$F(x, y, z, v, w) = \begin{bmatrix} xz + \kappa v \cos(w - y - C_p) \\ \alpha z + \kappa \frac{v}{x} \sin(w - y - C_p) \\ \frac{1}{T}[P - z - (1 + 2z)x^2] \end{bmatrix} \tag{5.18}$$

where x, y, z, v, w denote its five arguments. As for a steady state, the linearization of F can be written in the form of Eq. (5.2) as

$$DF\, q = A_1\, q(t) + A_2\, q(t-\tau)\,. \tag{5.19}$$

The matrices A_1 and A_2 can be computed as (compare Eq. (5.3))

$$A_1 = \begin{bmatrix} N_s & -\kappa R_s \sin(\omega_s\tau + C_p) & R_s \\ \frac{\kappa}{R_s}\sin(\omega_s\tau + C_p) & -\kappa\cos(\omega_s\tau + C_p) & \alpha \\ -\frac{2}{T}(1 + 2N_s)R_s & 0 & -\frac{1}{T}(1 + 2R_s^2) \end{bmatrix} \tag{5.20}$$

and

$$A_2 = \begin{bmatrix} -N_s & \kappa R_s \sin(\omega_s\tau + C_p) & 0 \\ -\frac{\kappa}{R_s}\sin(\omega_s\tau + C_p) & \kappa\cos(\omega_s\tau + C_p) & 0 \\ 0 & 0 & 0 \end{bmatrix}. \tag{5.21}$$

The block form of A_2 indicates that the N-equation Eq. (5.9) of the LK equations does not have a delay term. The matrix

$$\Delta(\lambda) := \lambda I - A_1 - A_2 e^{-\lambda\tau}$$

gives rise to the characteristic equation as $\det(\Delta(\lambda)) = 0$. As was mentioned in Sec. 5.1.3, the variational equation has T-periodic coefficients in general. However, neither A_1 nor A_2 have periodic coefficients. Therefore, the characteristic equation is autonomous, as one would expect from a steady state. This is a direct consequence of the S^1-symmetry of the ECMs. The characteristic equation can be calculated as

$$\begin{aligned} 0 \;=\;& \lambda^3 \\ &+ [\frac{1}{T}(1+2R_s^2) - 2N_s(1-e^{-\lambda\tau})]\,\lambda^2 \\ &+ [\frac{2R_s^2}{T}(1+2N_s) + \kappa^2(1-e^{-\lambda\tau})^2 + \frac{2\kappa}{T}\cos(\omega_s\tau + C_p)(1+2R_s^2)(1-e^{-\lambda\tau})]\,\lambda \\ &+ \frac{\kappa^2}{T}(1+2R_s^2)(1-e^{-\lambda\tau})^2 \\ &+ \frac{2\kappa R_s^2}{T}(1+2N_s)(\cos(\omega_s\tau + C_p) - \alpha\sin(\omega_s\tau + C_p))(1-e^{-\lambda\tau}) \end{aligned} \tag{5.22}$$

where R_s, ω_s and N_s of the ECM under consideration are given by Eqs. (5.12)–(5.14). (We remark that Eq. (5.22) corrects some minor errors in (the derivation of) the characteristic equation presented in Ref. [63].)

Equation (5.22) is an implicit, transcendental equation that contains all stability information of the ECMs. Note that $\lambda = 0$ is always an eigenvalue (corresponding to the trivial Floquet multiplier of the ECM). If Eq. (5.22) has an additional eigenvalue $\lambda = 0$ then a saddle-node bifurcation takes place. If it has a complex pair of λ with zero real part then an ECM undergoes a Hopf bifurcation. The respective solution branches can best be found by continuation in the spirit of bifurcation theory.

Linear stability analysis of ECMs, that is, computing regions of different numbers of ECMs and the curve of the first Hopf bifurcation, is a well established technique that has been applied to different types of lasers (given by sets of laser parameters in Eqs. (5.8) and (5.9)). Figure 5.4, reproduced from the survey paper Ref. [60], shows such regions in the (C_p, κ)-plane.

A bifurcation analysis of the characteristic equation in the regime of moderate delays was recently performed by Wolfrum and Turaev in their paper Ref. [69]. They pay particular attention to the condition that there are two ECMs with the same inversion N_s but different ω_s. This is called the Petermann-Tager condition, because Petermann and Tager observed that near such a point one can find oscillations of the laser at a frequency that is given by the difference of the two ECMs involved. This was later confirmed, by asymptotic methods and by numerical continuation with DDE-BIFTOOL [13, 30, 49, 50]; these continuation results are discussed in the next section. In the (ϕ, η)-plane shown in Fig. 5.5 (the $(C_p, \kappa\tau)$-plane in our notation) a curve of Petermann-Tager points (denoted PT) emerges from a mode degeneracy point MD on the saddle-node curve. Apart from the oscillations associated with the curve PT, there is also a second type of oscillations

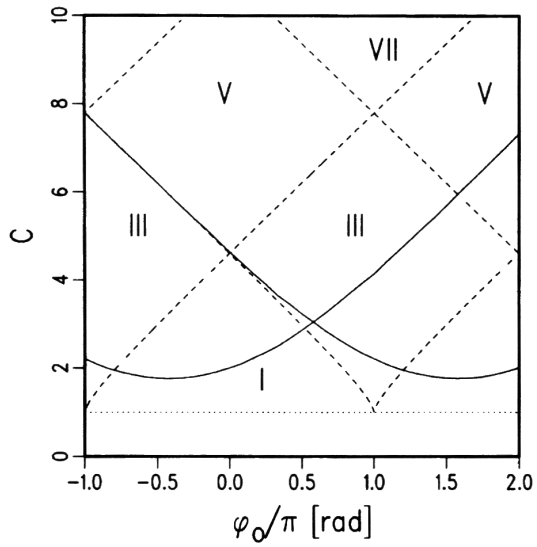

Figure 5.4: Regions in the (φ_0, C)-plane (the (C_p, κ)-plane in our notation) with an indication of the maximal number of ECM that may occur (roman numerals). The saddle-node bifurcation curves are dashed and the Hopf bifurcation curve is a solid curve. (The Hopf curve has two parts, which match up by identifying 0 with 2π; the dotted line is the lower boundary for possible multiple solutions.) Reproduced from G.H.M. Van Tartwijk and D. Lenstra, *Quantum Semiclass. Opt.* 7 (1995) 87–143 ©1995 by Institute of Physics Publishing.

with a frequency close to the relaxation oscillation frequency of the solitary laser; the authors call it dispersive self Q-switching (DQS) pulsations due to their similarity with pulsations in two-section DFB lasers. The Hopf bifurcation condition is derived from the characteristic equation (the equivalent of Eq. (5.22)) and analyzed by scaling methods in the limit of small $\varepsilon = \tau/T$. Good agreement is found between these theoretical results and a numerical continuation of the Hopf bifurcation condition; see Fig. 5.5 where the DQS Hopf curve is in good agreement with the asymptotic dashed curves emerging from the point MD of mode degeneracy.

A full bifurcation analysis of the characteristic equation Eq. (5.22) has not been performed. The next step of presenting a geometrical picture of the bifurcation set in (C_p, κ, P)-space of all bifurcations of ECMs is the topic of an ongoing project. This bifurcation set can be seen as the 'ECM-backbone' of the COF laser, and it will be presented elsewhere.

5.3.4 Continuation near connecting bridges

The numerical continuation study of the LK equations by Haegeman et al. in Ref. [30] is a good representation of the state-of-the-art in numerical bifurcation analysis of the COF laser. In this section (a number of) their results are reviewed. The authors are considering the LK equations in the exact same form as Eqs. (5.8) and (5.9) but use $\omega_o\tau$ instead of C_p. The starting point of their analysis is the realization that when different branches

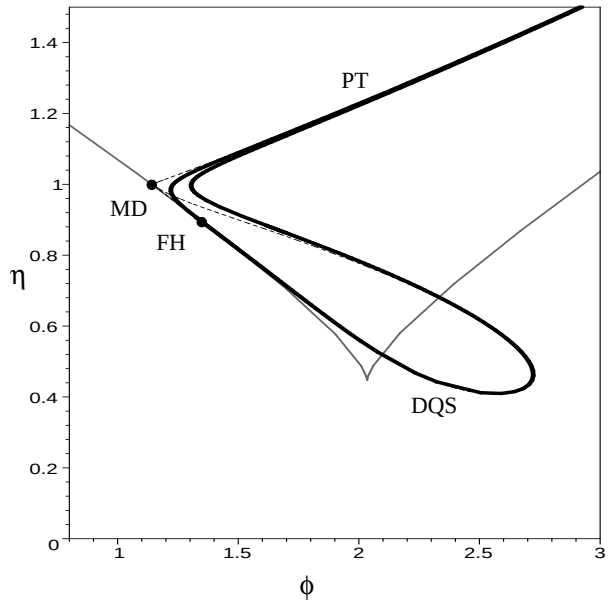

Figure 5.5: Numerically computed Hopf curve (thick curve) in the (ϕ, η)-plane (the $(C_p, \kappa\tau)$-plane in our notation) and the asymptotic approximation (dashed curves) in the limit of small $\varepsilon = \tau/T$. Reproduced from M. Wolfrum and D. Turaev, *Opt. Commun.* 212 (2002) 127–138 ©1995 by Elsevier Science.

of ECMs cross (as a function of κ) and have the same inversion N_s then there should be periodic orbits with a frequency given by the frequency difference of the involved ECMs. This was the observation of Petermann and Tager mentioned in the previous section.

As was shown in Ref. [50], in the limit of small $\varepsilon = 1/T$ this gives rise to mixed mode solutions for the electric field of the form

$$E(t) = A_1 \exp[i(\Delta_1 - C_p)t] + A_2 \exp[i(\Delta_2 - C_p)t]$$

where Δ_1 and Δ_2 are the frequencies of the two ECMs and A_1 and A_2 are their amplitudes. As a consequence, the power $|E|^2$ oscillates at the frequency $|\Delta_1 - \Delta_2|$. These mixed mode solutions survive in the case of nonzero ε and give rise to what are called bifurcation bridges in Ref. [30]. They are in fact branches of tori connecting Hopf bifurcation points on different branches of ECMs.

In order to study this phenomenon by continuation with DDE-BIFTOOL one first needs to take into account the S^1-symmetry of the LK equations. The reason is that DDE-BIFTOOL, like any continuation software, requires isolated solutions. This was achieved in Ref. [30] by introducing a new phase parameter b by setting $E(t) = A(t)e^{ibt}$ where $A(t)$ is also complex. With this ansatz it is possible to remove the indeterminacy due to the symmetry group by fixing the phase of $A(t)$ and solving for the associated unkown value b_s of the new variable b. Then an ECM corresponds to an equilibrium of this extended system with the same expression for its stability (because the ϕ-direction is neutral at an ECM). What is more, quasiperiodic solutions (that is, tori) can now be continued as periodic solutions of this extended system. This makes it possible to compute the tori that form the bridges between different branches of ECMs as periodic orbits; see

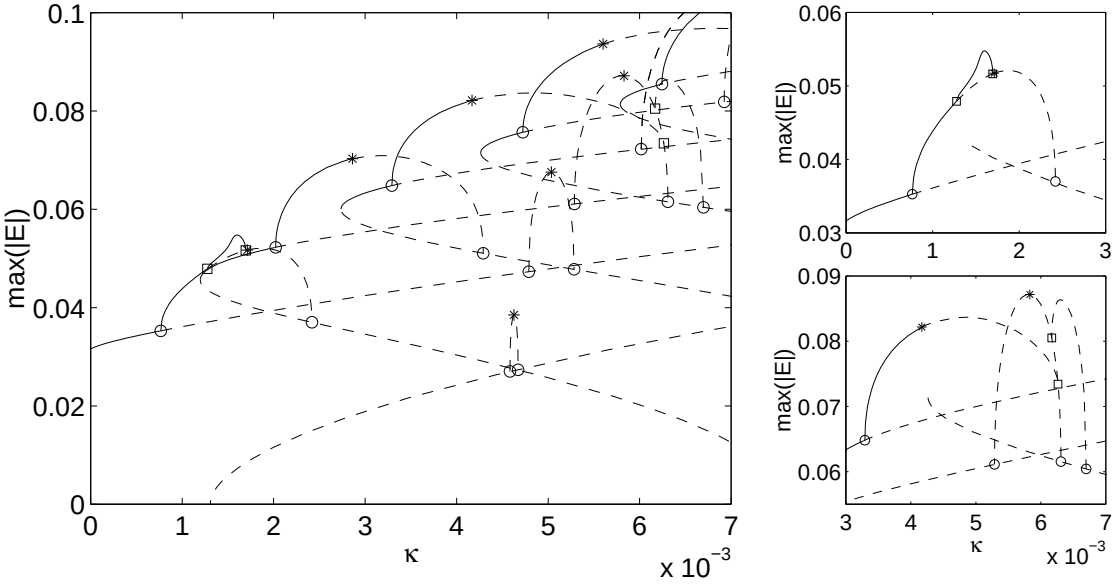

Figure 5.6: Bifurcation bridges connecting different branches of ECMs of the LK equations; dashed curves correspond to unstable solutions, the two right panels are enlargements. Reproduced from B. Haegeman, K. Engelborghs, D. Roose, D. Pieroux, and T. Erneux, *Phys. Rev. E* 66 (2002) 046216 ©2002 by the American Physical Society.

Ref. [30] for details.

Figure 5.6 (a) shows a number of branches of ECMs that are born in saddle-node bifurcations (seen as the left-hand fold points). As was mentioned earlier, one of the ECMs (the mode) is initially stable and the other (the anti-mode) is not. Both modes and the anti-modes undergo Hopf bifurcations. Branches that cross each other are connected by bridges of periodic orbits (or rather tori); Fig. 5.6 (b) and (c) shows two enlargements. The periodic orbits generating the bridges generally undergo further bifurcations, either period-doubling or torus bifurcations, and this generally leads to regions of chaotic dynamics [47] (not shown in the figure).

The paper Ref. [30] also studies the dependence of the connecting bridges on the parameters α and C_p, showing that they may 'rupture', meaning that the connection is lost in further bifurcations. Shown here are only their results of the dependence on the feedback phase C_p, because they fit nicely into our earlier discussion.

Figure 5.7 (a) shows curves of saddle-node bifurcations (solid) and of Hopf bifurcations (dashed) bounding regions of stability of ECMs in the (C_p, κ)-plane. From the point p_2 two curves of pitchfork bifurcations emerge. At this bifurcation the radius of an ECM goes to zero (which corresponds to a Hopf bifurcation of the trivial equilibrium). Figure 5.7 (b) shows bifurcation curves of periodic orbits in the (C_p, κ)-plane. In the grey region the periodic solution corresponding to the first bifurcation bridge is stable. It is bounded by the Hopf bifurcation curve from Fig. 5.7 (a) and by curves of period-doubling bifurcations. Note how Figs. 5.4 and 5.5 capture the respective aspects of Figs. 5.7 (a) and (b).

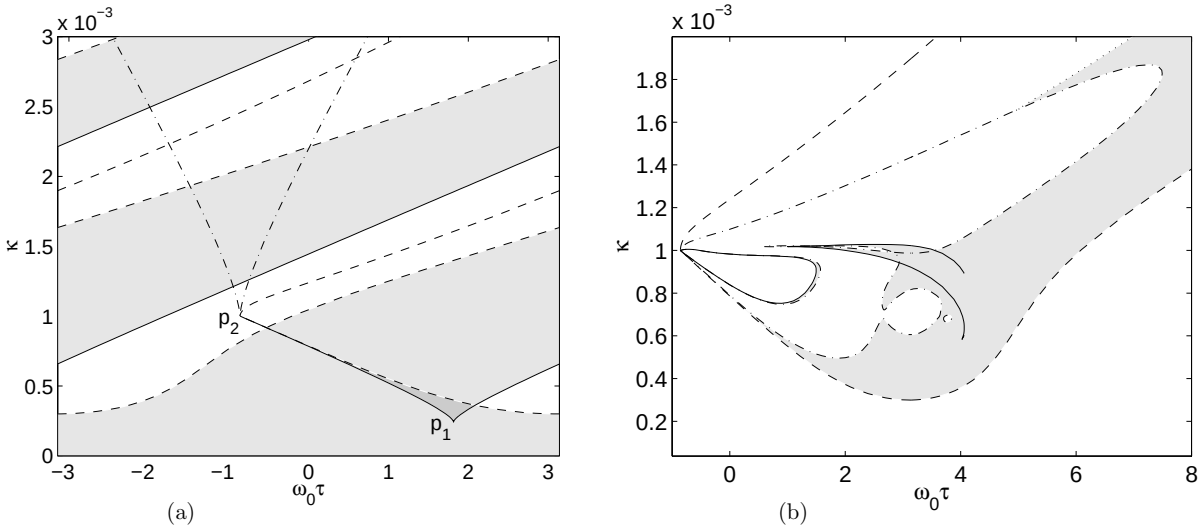

Figure 5.7: Panel (a) shows a bifurcation diagram in the (C_p, κ)-plane (note that $\omega_0\tau = C_p$) of ECMs of the LK equations; shown are curves of saddle-node bifurcations (solid), Hopf bifurcations (dashed) and pitchfork bifurcations (dot dashed). Panel (b) shows a bifurcation diagram in the (C_p, κ)-plane of periodic orbits of the LK equations; shown are curves of saddle-node bifurcations of periodic orbits (solid), Hopf bifurcations (dashed), period-doubling bifurcations (dot dashed) and torus bifurcations (dotted), and C_p is not taken modulo 2π. Reproduced from B. Haegeman, K. Engelborghs, D. Roose, D. Pieroux, and T. Erneux, *Phys. Rev. E* 66 (2002) 046216 ©2002 by the American Physical Society.

5.3.5 Global bifurcations of ECMs

A periodic orbit born in a Hopf bifurcation of an ECM first 'surrounds' only this ECM, a notion that makes sense because a Hopf bifurcation is an inherently two-dimensional phenomenon: close to the Hopf bifurcation the bifurcating periodic orbit is (in very good approximation) a nice round circle in a plane. (More technically, the Hopf bifurcation takes place in a two-dimensional centre manifold.) As κ is increased, there appear periodic orbits 'surrounding' several ECMs (in certain projections). The process of going from one situation to the other is sometimes called glueing, and it generally involves homoclinic bifurcations. Indeed it has been known for some time that homoclinic bifurcations occur in the LK equations. An example of a homoclinic orbit of an ECM with a one-dimensional unstable manifold and a two-dimensional strongest stable direction with complex conjugate eigenvalues (a saddle-focus) is shown in Fig. 5.8 (a) and (b). The ECM involved in the homoclinic bifurcation is an anti-mode shortly after its emergence in a saddle-node bifurcation (so that the unstable manifold is indeed one-dimensional). The periodic orbit is born in a Hopf bifurcation of the ECM that it surrounds in Fig. 5.8 (b). The homoclinic orbit was found by simulation as a large-period periodic orbit. Also in Ref. [30] the authors find homoclinic orbits (some also of saddle-focus type) by continuing periodic orbits to large period, and they show that the 'rupture' of bifurcation bridges is due to homoclinic bifurcations.

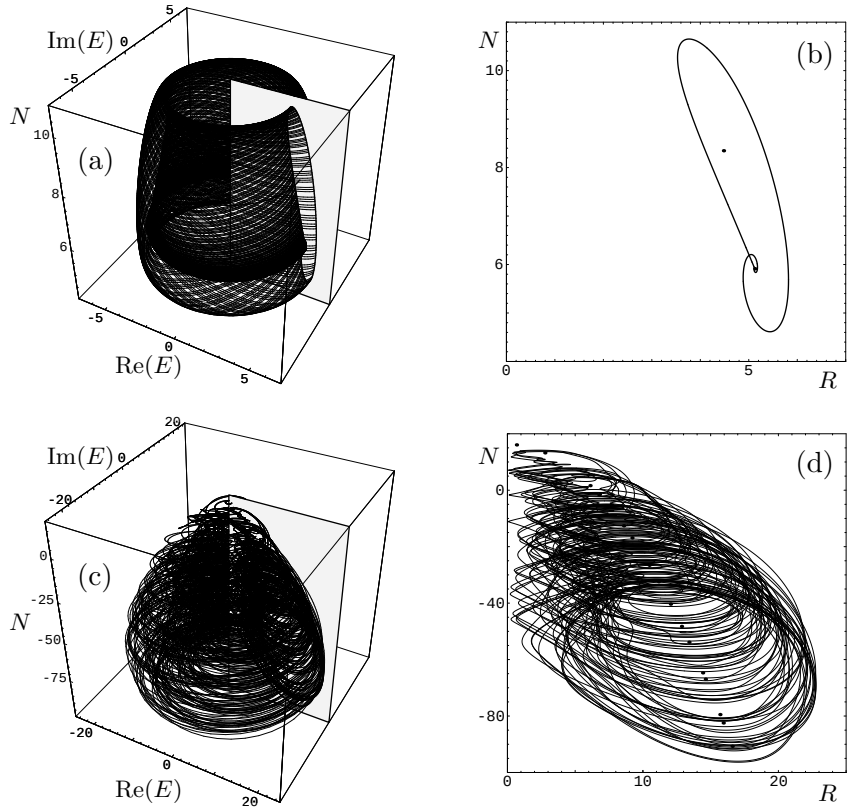

Figure 5.8: A homoclinic orbit to a saddle focus ECM in (E, N)-space (a) and in the (R, N)-plane (b), and an example of complicated dynamics surrounding several ECMs in (E, N)-space (c) and in the (R, N)-plane (d). The parameters are $\alpha = 10$, $\gamma = 2.55 \times 10^{-3}$, $A = 4.96 \times 10^{-7}$, $\tau = 714.3$, and $\kappa = 0.7313236 \times 10^{-3}$ in panels (a) and (b), and $\kappa = 5.6 \times 10^{-3}$ in panels (c) and (d) for the LK equations in the form given in Ref. [63].

The main challenge is to study the sequence of global bifurcations, homoclinic and heteroclinic, that lead to complicated dynamics with the aim to characterize the exact nature of the well-known low-frequency fluctuations (LFF); see Chapters 2 and 4. An example of complicated dynamics is shown in Fig. 5.8 (c) and (d). The attractor, which seems to be chaotic, 'surrounds' a number of ECMs. However, in terms of complexity this dynamics is still quite far from full blown LFF when the laser has hundreds or even thousands of ECMs. Neverthetheless, even the exact bifurcation transition from Fig. 5.8 (b) to (d) is not understood.

This section on the COF laser now finishes with some recent results [34] on how the study of 1D unstable manifolds of ECMs can cast some light on the nature of bifurcations as C_p is changed in the case of a short cavity (of the order of a few centimeters) as studied recently in Ref. [32]; see also Chapter 4. Figure 5.9 shows antimodes (denoted by $+$) and modes (denoted by $\circ$) and one branch of the 1D unstable manifold of one of the antimodes. This branch was computed by integrating from an initial condition close to the ECM along its linear unstable eigendirection. (Because of the S^1-symmetry, this can be

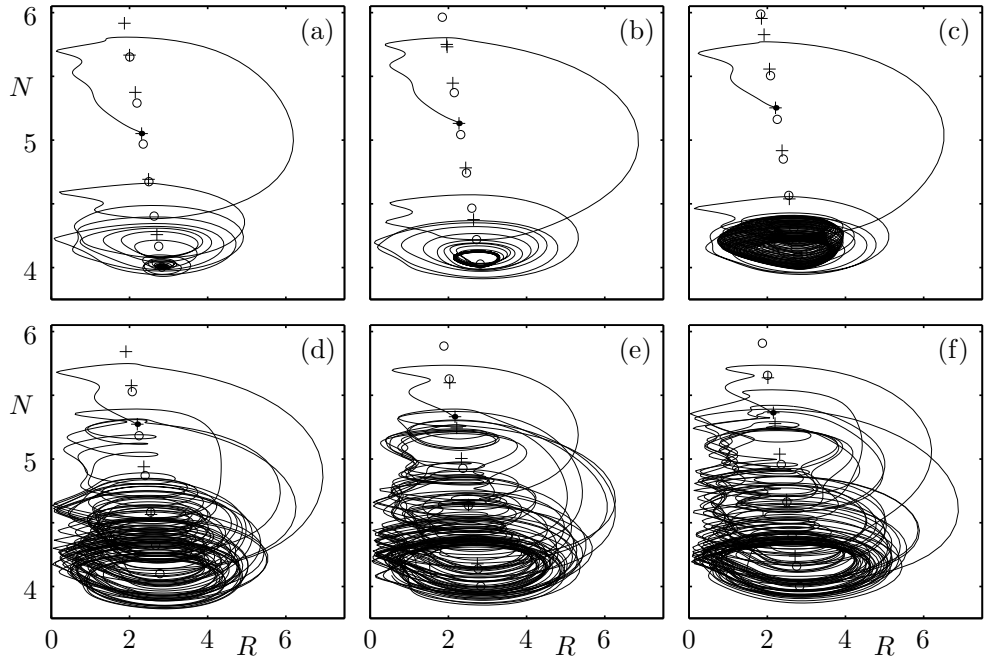

Figure 5.9: One branch of the 1D unstable manifold of a saddle ECM (anti-mode) in the short cavity regime, shown in panels (a) to (d) for decreasing values of C_p in projection onto the (R, N)-plane. From (a) to (f) C_p takes the values 24.98, 23.48, 21.13, 20.73, 19.56, and 18.93, where the LK equations and the other parameters are as in Ref. [34].

done like for a steady state as was explained in Sec. 5.2.3.) The branch initially ends up at a stable ECM (a), and then at increasingly complicated attractors as C_p is increased, namely a periodic orbit (b), torus (c) and chaotic attractors of increasing sizes; see panels (d) to (f). The dynamics on the attractor in Fig. 5.9 (f) is in fact very regular and has been called *pulse packages* [32]. An important feature of the branch is a mechanism of reinjection: the branch first visits a region of higher inversion N and then quickly extends all the way to the region of low N (or high gain). This produces an initial pulse in the laser power. There appear to be a number of global bifurcations in which the attractor increases in size, 'surrounding' more and more ECMs. The pulse packages themselves become more regular, which is seemingly due to the appearance of a quite narrow 'channel of reinjection' through which the trajectory travels at the beginning (producing the first and largest pulse) of each pulse package. This forces the pulse packages to be more alike until they finally disappear in a sudden transition back to constant laser output. The scenario in Fig. 5.9 agrees well with experimental measurements reported in Ref. [32]; see Ref. [34] for details.

5.4 Bifurcations in the PCF laser

Semiconductor lasers with phase-conjugate feedback (PCF) from a phase conjugating mirror (PCM) have received considerable attention because they have a number of positive properties. Due to the reversal of the light front in the PCM, the reflected wave travels back along the same path as the incident wave, meaning that alignment of the mirror is less of an issue. Furthermore, perturbations on the way to the PCM are undone on the way back, resulting in potentially more stable operation.

The main technical difficulty is realising a PCM. Phase conjugation can be achieved by a number of nonlinear optical processes, including stimulated Brillouin scattering, backward stimulated Raman scattering and three-wave down conversion [17]. Probably the most common process is degenerate four-wave mixing in which three input waves mix to produce a fourth output wave. Two of the input waves are counter-propagating pump waves of a given frequency, for example, from additional semiconductor lasers. The incident wave is the third wave, that enters the medium at any angle to the pump waves and is coupled to the pump waves through a third-order susceptibility $\chi^{(3)}$. This results is a fourth wave, which is phase-conjugated to the incident wave; see Chapter 3 for more introductory information.

Phase conjugate feedback may produce a highly focused beam [17], which is of considerable advantage when stable output is desired. The main application is mode locking [20] and phase locking, where PCF has been shown to reduce the laser noise considerably [1, 21, 60]. However, many other dynamical regimes have been identified, including periodic and quasiperiodic output, as well as chaotic dynamics; see, for example, Refs. [1, 17, 21, 38].

As is the case with the COF laser, the PCF laser can be modelled by a well-established rate equation for the evolution of the slowly varying complex electric field $E(t)$ and the population inversion $N(t)$ [21, 38], which can be written in the form

$$\begin{aligned} \frac{dE}{dt} &= \frac{1}{2}\left[-i\alpha G_N(N(t)-N_{\text{sol}}) + \left(G(t)-\frac{1}{\tau_p}\right)\right]E(t) \\ &\qquad +\kappa E^*(t-\tau)\exp[2i\delta(t-\tau/2)+i\phi_{\text{PCM}}] \end{aligned} \tag{5.23}$$

$$\frac{dN}{dt} = \frac{I}{q} - \frac{N(t)}{\tau_e} - G(t)\,|E(t)|^2\,. \tag{5.24}$$

In Eqs. (5.23) and (5.24), nonlinear gain is included as $G(t) = G_N(N(t)-N_0)(1-\epsilon P(t))$, where $\epsilon = 3.57\times10^{-8}$ is the nonlinear gain coefficient and $P(t) = |E(t)|^2$ is the intensity. Parameter values are set to realistic values corresponding to a Ga-Al-As semiconductor laser [21, 38] as summarized in Table 5.1, where $N_{\text{sol}} = N_0 + 1\,/\,(G_N\tau_p)$.

As is common in the field [21, 38], the constant phase shift at the PCM and the detuning parameter were both set to zero, so that the feedback term in Eqs. (5.23) and (5.24) reduces to $\kappa E^*(t-\tau)$. The main bifurcation parameter is the effective feedback strength $\kappa\tau$ (a dimensionless parameter), and in two-parameter investigations also the pump current I (in units of ampere) is varied.

The modelling assumptions here are, as for the LK equations, that the laser operates in single mode and the feedback is weak (because again only a single roundtrip in the

symbol	parameter	value
α	line-width enhancement factor	3.0
G_N	optical gain	$1190\,\mathrm{s}^{-1}$
τ_p	photon lifetime	1.4 ps
q	magnitude of the electron charge	1.6×10^{-19}C
τ_e	electron lifetime	2 ns
N_0	transparency electron number	1.64×10^8
τ	external cavity round-trip time	2/3 ns
ϕ_{PCM}	constant phase shift at PCM	0.0
δ	detuning parameter	0.0

Table 5.1: Parameter values of the PCF laser as modelled by Eqs. (5.23) and (5.24).

external cavity is taken into account). However, there is the further assumption that the PCM is so fast that the phase-conjugation can be modelled as instantaneous. The effect of non-instanteneous PCF has been considered in Refs. [4, 58]. As the interaction time in the PCM is increased from zero (the instantaneous case), the dynamics of the PCF laser is affected first for larger and then for lower and lower values of $\kappa\tau$. For the moderate values of $\kappa\tau$ near and just above the locking region (of steady state operation; see Sec. 5.4.2) of the PCF laser used in the results below, the dynamics is essentially unaffected when the interaction time in the PCM does not exceed 0.1 ns, which appears to be achievable with semiconductor PCMs; see Ref. [4] and also Chapter 3.

The general picture of the dynamics that emerged from earlier studies by numerical simulation is that there are windows where the PCF laser has stable periodic orbits, also called external cavity modes (ECMs) of the PCF laser [1, 21, 38]. When the laser operates at an ECM then it produces periodic output at a frequency that is very close to a multiple of the external roundtrip frequency. Different ECMs are separated from each other by 'bubbles' of more complicated dynamics, including regions of chaos. The transitions through these bubbles can be interpreted as a competition in the laser between neighbouring ECMs; see Refs. [21, 38] for more details.

The PCF laser is a second laser system that has been studied recently with new methods from bifurcation theory [24, 25, 26, 28], and this is summarized in the next sections. The question is how the laser changes its behaviour as parameters are changed. The main bifurcation parameters are the effective feedback strength $\kappa\tau$ and the pump current I. A detailed two-parameter bifurcation diagram near the locking region is presented in the $(\kappa\tau, I)$-plane. Furthermore, it is shown how unstable manifold computations can be used to understand a transition to chaos via the break-up of a torus.

5.4.1 Symmetry of the PCF laser equations

In contrast to the LK equations, Eqs. (5.23) and (5.24) are symmetric under the discrete $\mathbb{Z}_2$-symmetry given by the transformation $(E, N) \to (-E, N)$. In other words, the symmetry group is generated by a rotation over π of the complex E-plane, which is physically a phase shift of the electric field by π. A consequence of this symmetry is that any at-

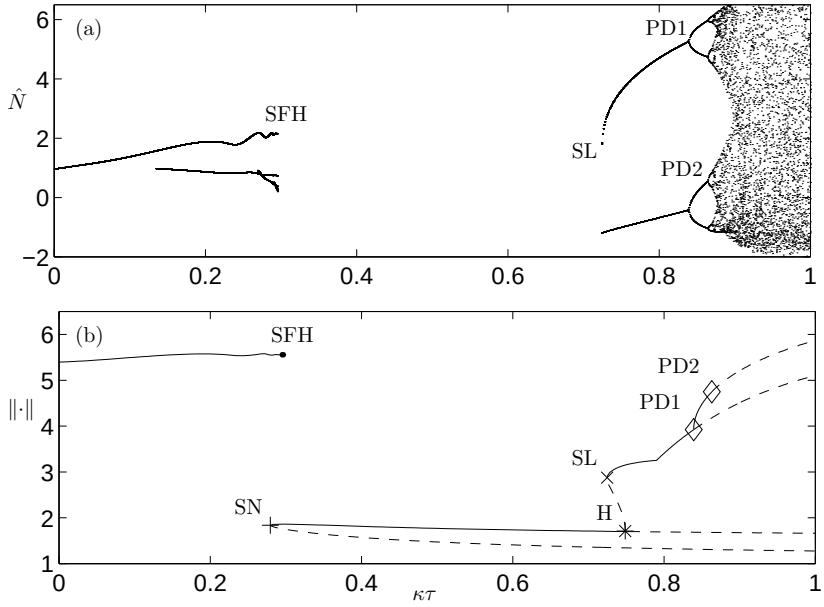

Figure 5.10: The bifurcation diagram of the PCF laser Eqs. (5.23) and (5.24) near the locking region, obtained by simulation showing normalised inversion $\hat{N}$ versus the feedback strength $\kappa\tau$ (a), and computed by continuation with DDE-BIFTOOL showing a normalised amplitude versus $\kappa\tau$ (b). The pump current was set to $I = 65.1\,\mathrm{mA}$. Reproduced from K. Green and B. Krauskopf, *Phys. Rev. E* 66 (2002) 073207 ©2002 by the American Physical Society.

tractor (or other invariant set) is either symmetric, or has a symmetric counterpart. This allows for symmetry-breaking and symmetry-restoring bifurcations; see Refs. [26, 38]. For example, when a symmetric periodic orbit has a Floquet multiplier +1 then it may undergo a symmetry-breaking bifurcation instead of a saddle-node bifurcation. Furthermore, a symmetric periodic orbit cannot undergo a period-doubling bifurcation [44].

Because the symmetry group of the PCF laser is discrete, solutions are isolated (that is, they do not occur as solution families as for the COF laser). This means that DDE-BIFTOOL can be used without any modification to find and continue equilibria and periodic orbits.

5.4.2 Bifurcation diagram near the locking region

As was mentioned, an important motivation for using PCF is to achieve stable locked laser output. This type of dynamics occurs in the laser locking region. The question arises of what happens at the boundaries of the locking region. The bifurcation diagram in Fig. 5.10 (a) was obtained by numerical simulation and it shows the normalised value of the inversion $\hat{N} = (N/N_{sol} - 1) \times 10^3$ whenever the intensity P crosses its average value in the positive direction. The locking region is the region without any points, while a small number of points corresponds to a periodic orbit and a large number of points to chaotic dynamics. The dynamics for $\kappa\tau \in [0.0000, 0.2953]$ was computed for increasing

$\kappa\tau$ and that for $\kappa\tau \in [0.7487, 0.9004]$ for decreasing $\kappa\tau$. This is due to small hysteresis loops caused by bistabilities at the boundaries of the locking region that are discussed below.

Figure 5.10 (b) was obtained by numerical continuation with the package DDE-BIFTOOL. Plotted is the real part E_x of the steady states, and $|\max(E_x) - \min(E_x)|$ (offset by the E_x-value of the steady states at the Hopf point) for periodic orbits. Attracting solutions are drawn as solid curves and unstable ones as dashed curves. Figure 5.10 (b) gives more information than Fig. 5.10 (a) in terms of the bifurcations taking place, because also followed are unstable solutions and their bifurcations. In terms of bifurcations of the stable equilibrium, the boundaries of the locking region are given by the saddle-node bifurcation *SN* at $\kappa\tau \approx 0.2794$ and the Hopf bifurcation *H* at $\kappa\tau \approx 0.7487$. There is a saddle-focus heteroclinic (or Shilnikov) bifurcation *SFH*, where the periodic orbit for small values of $\kappa\tau$ (the continuation of the free-running laser solution) is destroyed. This bifurcation takes place at $\kappa\tau \approx 0.2953$, that is, just *after SN* for increasing $\kappa\tau$, leading to a bistability between the locked state and a large periodic orbit. Similarily, there is a saddle-node bifurcation of limit cycles *SL* creating two pairs of symmetric periodic solutions at $\kappa\tau \approx 0.7247$, that is, *before* the Hopf bifurcation *H*. So at the right boundary of the locking region there is also a small region of bistability, this time between the locked state and a small periodic orbit. This stable periodic orbit then undergoes successive period-doublings, leading to a region of chaotic dynamics; see Fig. 5.10 (a). More details of this transition and phase portraits in (E, N)-space (obtained by computing the 1D unstable manifolds of the saddle equilibria) can be found in Ref. [24].

How typical is the transition in Fig. 5.10 when one considers different values of the pump current I? Or in other words, what is the bifurcation diagram in the two-dimensional $(\kappa\tau, I)$-plane? As was summarized in Sec. 5.2, the continuation of the bifurcations *SN*, *H* and *SFH* in the $(\kappa\tau, I)$-plane is possible with DDE-BIFTOOL, while the bifurcations *SL*, *PD* and *T* can at present only be detected but not continued.

Figure 5.11 shows the resulting 2D bifurcation diagram in the $(\kappa\tau, I)$-plane near the locking region, where the computations were started from the bifurcation points in Fig. 5.10 (b). The locking region is bounded on the left by the curve *SN* of saddle-node bifurcations and on the right by the (supercritical) left-most parts of the curves H_1 and H_2 of Hopf bifurcations. (The curves H_1 and H_2 are drawn dark when they are supercritical and lighter when they are subcritical.) The lower boundary of the locking region is given by a curve *PF* of pitchfork bifurcations. When this curve is crossed, the locked solution emerges from the trivial steady state as a pair of non-symmetric stable steady states, which constitutes the laser threshold in the PCF laser due to the $\mathbb{Z}_2$-symmetry of Eqs. (5.23) and (5.24).

Inside the locking region there is a curve *SFH*, the continuation of the saddle-focus heteroclinic orbit. This curve has been computed with the recent extension to DDE-BITOOL introduced in Ref. [52], the heteroclinic orbits along *SFH* are shown in Fig. 5.12. This curve *SFH* starts on the curve *SN* at a codimension-two noncentral saddle-node heteroclinic point *SNH* at $(\kappa\tau, I) \approx (0.225, 0.06433)$, and it ends at what is known as a *T-point* [18], indicated by *TP*, at $(\kappa\tau, I) \approx (2.177, 0.070394)$. (The point *SNH* is a saddle-node homoclinic bifurcation [44] when dividing out the $\mathbb{Z}_2$-symmetry of Eqs. (5.23) and (5.24).) Below *SNH* the saddle-node bifurcation along *SN* takes place on a periodic

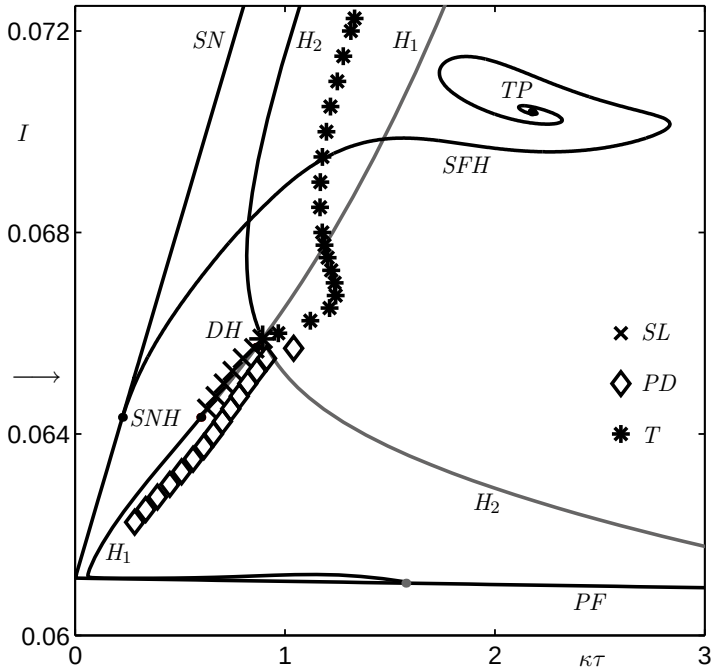

Figure 5.11: Bifurcation diagram in $(\kappa\tau, I)$-space near the locking region of the PCF laser Eqs. (5.23) and (5.24). The arrow corresponds to the one-parameter continuation for $I = 65.1\,\mathrm{mA}$ in Fig. 5.10.

orbit. The T-point is at the center of a spiral of the curve *SFH*, and at *TP* the heteroclinic connections between the two non-symmetric steady states are destroyed; see Ref. [18]. As can be seen in Fig. 5.12 (d), this happens because the heteroclinic connection passes closer and closer to the trivial equilibrium, eventually leading to two separate connections, one between a first non-symmetric equilibrium and the trivial equilibrium and a second one from the trivial equilibrium to the symmetric counterpart of the first non-symmetric equilibrium; see Ref. [28] for details.

In the region above the curve *SFH* and between *SN* and H_2 there is a bistability between a large periodic orbit and a pair of non-symmetric steady states, in agreement with our earlier discussion of the left locking boundary. The bistability on the right-hand boundary of the locking region mentioned earlier occurs in the small region bounded by the curves H_1 and *SL*. (Note that *SL* cannot be continued and was instead found at the values of I marked by the crosses.)

The point *DH* at $(\kappa\tau, I) \approx (0.893, 0.06589)$ where the curves H_1 and H_2 cross is a further codimension-two point called a double-Hopf bifurcation. At this point there is an equilibrium with two pairs of complex eigenvalues on the imaginary axis and it is known that the system can bifurcate to a number of invariant objects, including two-dimensional tori; see, for example, Refs. [29, 44]. It appears that near *DH* there is a switch from a period-doubling route to chaos (as observed in Fig. 5.10 (a)) to a route to chaos via the break-up of a torus. This is evidenced by the points *PD* and *T* that were found in the region of $\kappa\tau < 1.5$.

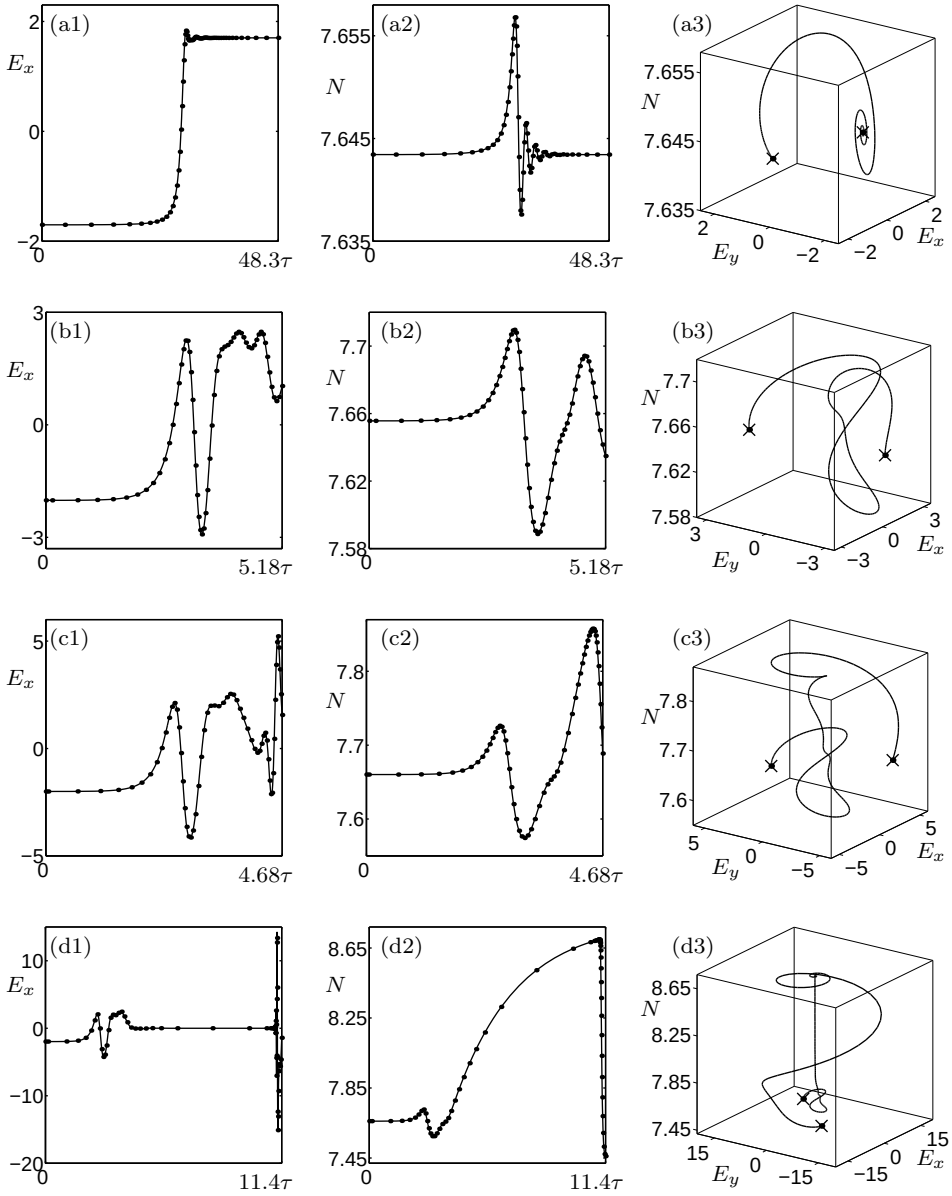

Figure 5.12: Heteroclinic orbits along the curve *SFH*; from (a) to (d) $(\kappa\tau, I)$ takes the values $(0.2533, 0.06467)$, $(1.5835, 0.06987)$, $(2.1141, 0.07050)$, and $(2.1767, 0.07039)$. Panel (d) shows the heteroclinic orbit at the point TP in Fig. 5.11. The first and second columns shows the E_x-profile and the N-profile over the time interval that was used in the computation, and the third column is a projection onto (E, N)-space.

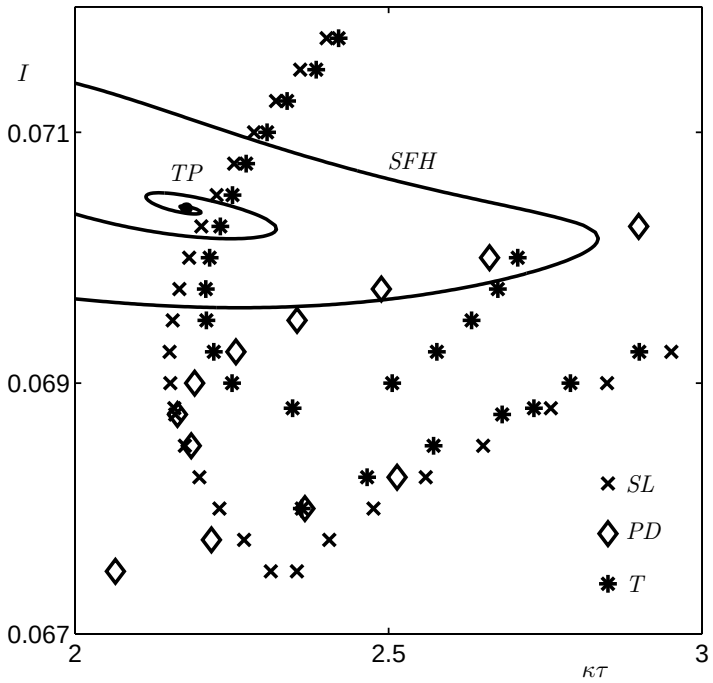

Figure 5.13: Bifurcation diagrams in $(\kappa\tau, I)$-space of periodic orbits originating from the Hopf curve H_2 in Fig. 5.11.

As is shown in Fig. 5.13, the periodic orbits bifurcating from the Hopf curve H_2 undergo further bifurcations in the region of $\kappa\tau > 2$. The situation is quite complicated. There is a region with a cusp bounded by saddle-node bifurcations of limit cycles *SL*. Along the curve *SL* a pair of periodic orbits bifurcates. Furthermore, there are points *PD* of period-doubling and *T* of torus bifurcations that appear to form nice curves. In the regions between the curves *SL* and *T* one finds extra stable periodic orbits. However, it is not entirely clear which points belong to which curve and where they start and end up. It is known that the different curves can interact at special points, such as 1:1 and 1:2 resonance points. This is not uncommon in laser systems; see, for example, Ref. [66]. The exact structure of these bifurcations will only be revealed when the continuation of the respective curves becomes available.

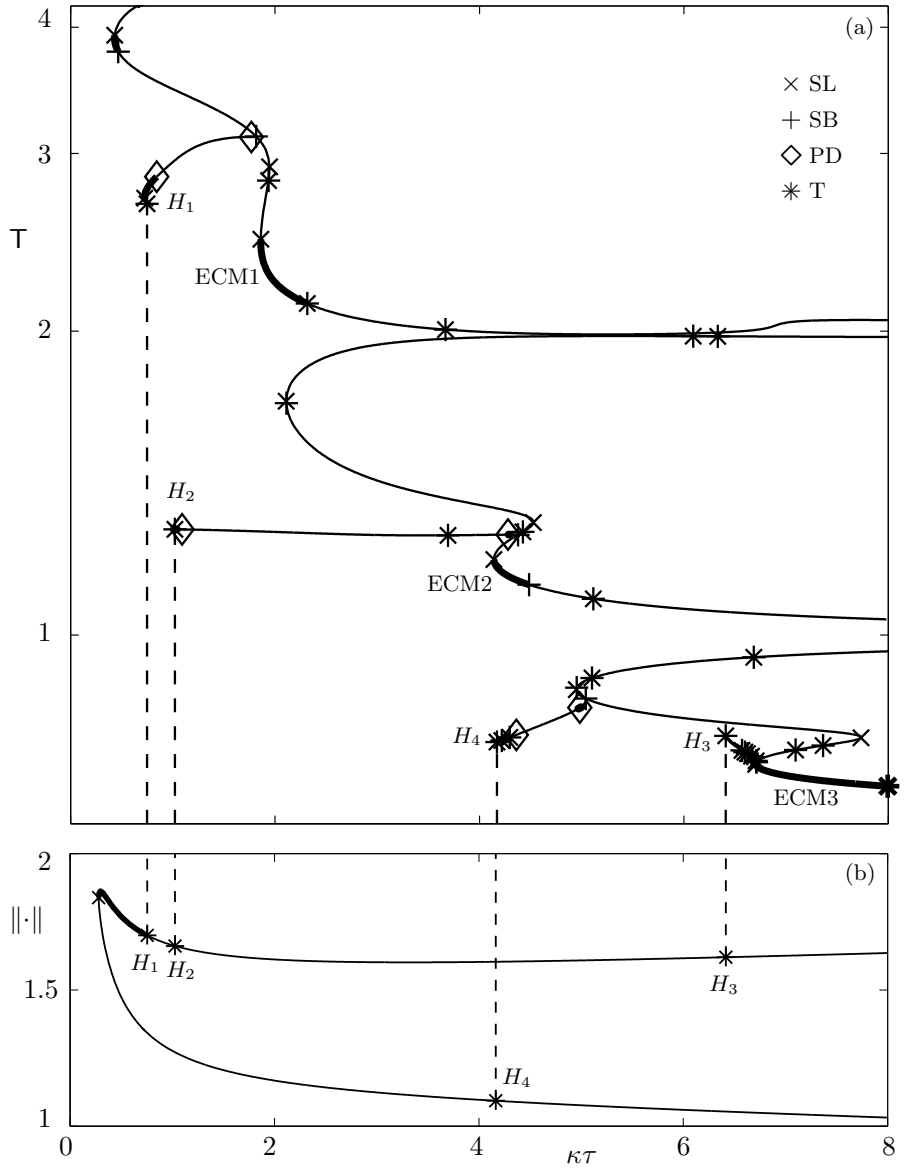

Figure 5.14: The ECMs of the PCF laser are connected to the steady state via curves of Hopf bifurcations. Panel (a) shows the continuation of periodic orbits, plotted as the period T versus $\kappa\tau$; panel (b) shows the continuation of the steady state, plotted as a normalised amplitude versus $\kappa\tau$; the pump current is $I = 65.1\,\mathrm{mA}$.

5.4.3 Bifurcations of ECMs

External cavity modes of the PCF laser are genuine periodic orbits of Eqs. (5.23) and (5.24). There are no analytic expressions for the ECMs or their stability, but they have been found and followed numerically; see Ref. [25] for details. Figure 5.14 shows the result of a bifurcation study with DDE-BIFTOOL in the parameter range $\kappa\tau \in [0.0, 8.0]$.

Panel (a) shows branches of periodic orbits; plotted is the period T along these branches and boldfaced parts of curve indicate that the periodic orbit is stable. The main branches are of symmetric periodic orbits and the three boldfaced parts correspond to the first three ECMs; the continuation was started from these ECMs, which were found by integration. As a consequence of the $\mathbb{Z}_2$-symmetry of Eqs. (5.23) and (5.24) a symmetric periodic orbit of period T corresponds to periodic output of the laser of period $\mathsf{T}/2$ [36]. Note that ECM1 to ECM3 correspond to power oscillations in the ranges 1.21–1.40 GHz, 2.51–2.67 GHz and 4.03–4.20 GHz, respectively, which is roughly at integer multiples of the external cavity frequency of c/L of the PCF laser [38]. Secondary branches of non-symmetric periodic orbits bifurcate at symmetry-breaking bifurcations. These branches end up at Hopf bifurcations, denoted H_1 to H_4.

Figure 5.14 (b) shows the branch of the non-symmetric steady state, which is also shown in Fig. 5.10 (b) in a smaller $\kappa\tau$ range. On this branch the Hopf bifurcations H_1 to H_4 are marked. The dashed vetical lines show that the points H_1 to H_4 are indeed the same points in both panels. Note that the points H_1 and H_2 are on the curves H_1 and H_2 in Fig. 5.11 at the indicated value of $I = 65.1\,\mathrm{mA}$.

Figure 5.14 shows that the ECMs are connected to the branch of steady state by branches of periodic orbits. In Ref. [11] this phenomenon was confirmed analytically in the singular limit of large $T = \tau_e/\tau_p$ of Eqs. (5.23) and (5.24). There is in fact a complicated web of other branches of periodic orbits, some of which end up at homoclinic bifurcation points; see Ref. [25] for details.

5.4.4 Break-up of a torus and crisis bifurcation

There is a quite complex bifurcation scenario of a transiton to chaos via the break-up of an invariant torus in the PCF laser; for more details see Ref. [26]. It occurs in the range of $\kappa\tau \in [2.300, 2.800]$ as is shown in Fig. 5.15 with bifurcation diagrams obtained by simulation (a) and by numerical continuation of the locked periodic orbit (b).

Figure 5.15 (a) shows a stable periodic solution, namely the external cavity mode ECM1 from Fig. 5.14 (a), that loses its stability at $\kappa\tau \approx 2.307$. The dynamics on the bifurcating attracting torus is initially quasiperiodic or periodic with extremely high frequency. At $\kappa\tau \approx 2.441$ there is a saddle-node bifurcation of limit cycles SL where the dynamics on the torus becomes locked, as is evidenced by the five distinct branches in the bifurcation diagram. At $\kappa\tau \approx 2.556$ the locked periodic orbit itself loses its stability and bifurcates to a torus. This new torus corresponds to quasiperiodic modulations of the laser output, and is shaped like a 'hose' wrapped around the remainder of the initial locked solution. At $\kappa\tau \approx 2.570$ this new torus suddenly is replaced by a much larger chaotic attractor in a bifurcation that does not show any hysteresis. This is quite a spectacular change in the laser's output: a sudden transition from a periodic oscillation of the

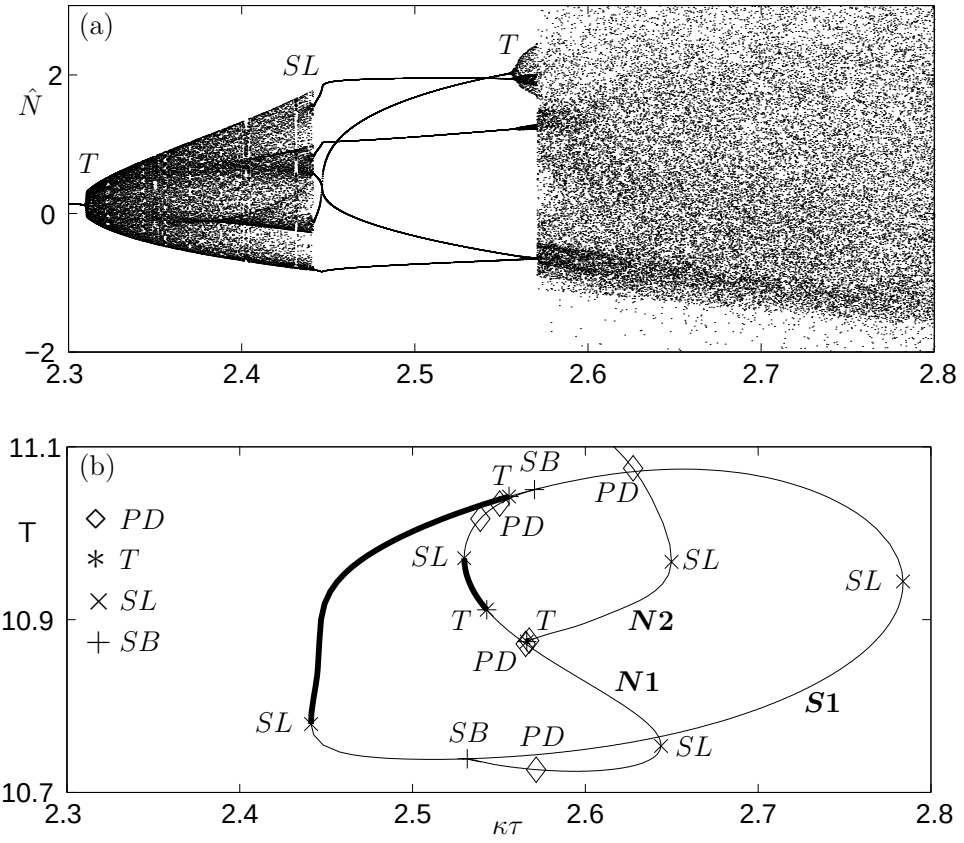

Figure 5.15: The bifurcation diagram of the PCF laser Eqs. (5.23) and (5.24) near the break-up of a torus, obtained by simulation showing normalised inversion $\hat{N}$ versus the feedback strength $\kappa\tau$ (a), and computed by continuation with DDE-BIFTOOL showing the period T versus $\kappa\tau$ (b). The pump current was set to $I = 65.1\,\mathrm{mA}$. Reproduced from K. Green and B. Krauskopf, *Physica D*, 173(1-2) (2002) 114–129 ©2002 by Elsevier Science.

power to a chaotic signal. Note that a similar scenario has been found in simulations of the LK equations in Ref. [47].

To shed more light on the bifurcations involved, Fig. 5.15 (b) shows a bifurcation diagram of the period T against $\kappa\tau$, obtained by continuation with DDE-BIFTOOL that was started from the stable locked periodic solution. The oval branch $\boldsymbol{S1}$ of symmetric periodic solutions is born and destroyed at the maximum and minimum values of $\kappa\tau$ in two saddle-node bifurcations of limit cycles SL. As is indicated by boldfacing, there is a stable locked solution in the interval $\kappa\tau \in (2.441, 2.556)$, the right endpoint of which is indeed a torus bifurcation. There are two more bifurcations on $\boldsymbol{S1}$, namely the two symmetry-breaking bifurcations denoted by SB. These two bifurcation points are connected by the branch $\boldsymbol{N1}$ of non-symmetric periodic orbits. There are further bifurcations along $\boldsymbol{N1}$, which we will not discuss here in detail. Note, however, that this branch $\boldsymbol{N1}$ features a window of stability between the points SL and T in the range $\kappa\tau \in (2.530, 2.543)$; for details see Ref. [26].

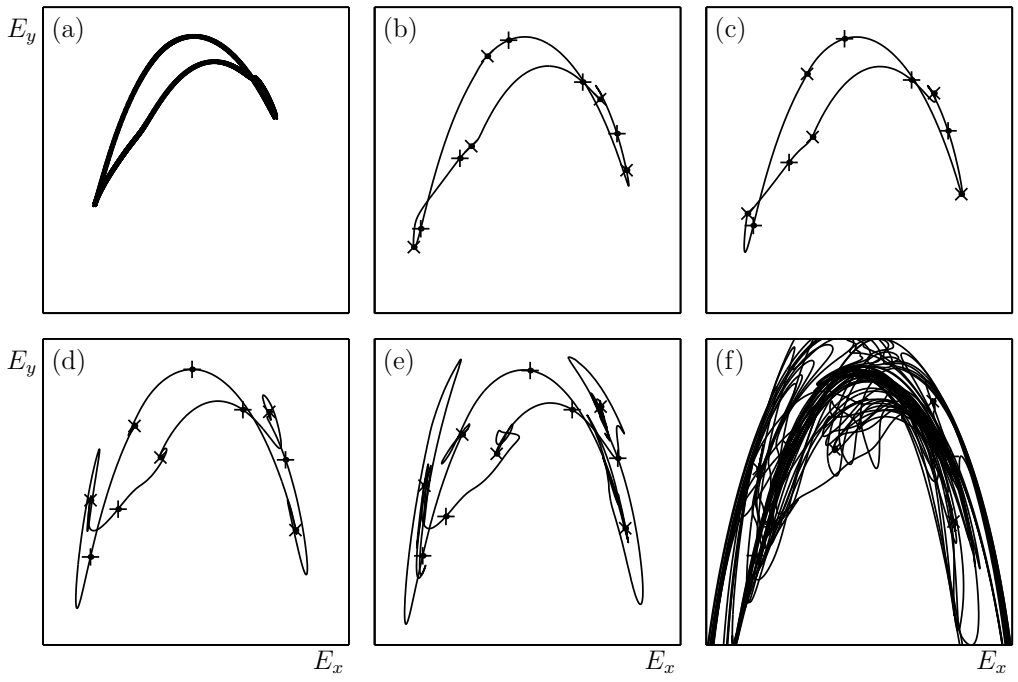

Figure 5.16: Break-up of the torus of the PCF laser (see text for details); from (a) to (f) $\kappa\tau$ takes the values 2.400, 2.445, 2.450, 2.480, 2.500 and 2.531; the region shown is $E \in [-300, 300] \times [140, 300]$ and $I = 65.1\,\mathrm{mA}$. Reproduced from K. Green and B. Krauskopf, *Physica D*, 173(1-2) (2002) 114–129 ©2002 by Elsevier Science.

While the bifurcation diagrams in Fig. 5.15 give a clear indication that one is dealing with a transition to chaos via the break-up of a torus, it is crucial to look at what happens to the torus itself when one wants to understand the exact nature of the sudden transition to a large chaotic attractor.

To this end Fig. 5.16 shows the 1D unstable manifolds of the saddle periodic orbit in the locking region (which corresponds to the lower part of the branch ***S1*** in Fig. 5.15(b)). This orbit intersects a suitable plane $\Sigma \equiv \{N = 7.620 \times 10^8\}$ in four clusters of five points, of which one cluster corresponding to one of the four intersections of the torus with Σ is shown. Each of the five points comes with its history of length τ and is a fixed point of the Poincaré return map defined by Σ. The 1D unstable manifolds of these five points, which are indicated by crosses (+) in Fig. 5.16, were computed with the method explained in Sec. 5.2.3. It is important to remember that shown is a two-dimensional projection of an infinite-dimensional system; in particular, branches of 1D unstable manifolds are allowed to intersect each other.

Figure 5.16 reveals that the torus is smooth immediately after locking (b) and resembles the unlocked torus (a), as is to be expected from general theory. Indeed all branches of the manifolds connect smoothly at the attracting periodic points (×). At $\kappa\tau \approx 2.4502$ the torus loses its smoothness because the branches now start to spiral into the attractors (c). This is due to them developing two complex conjugate Floquet multipliers, as was confirmed with DDE-BIFTOOL. In terms of the laser's dynamics, this corresponds

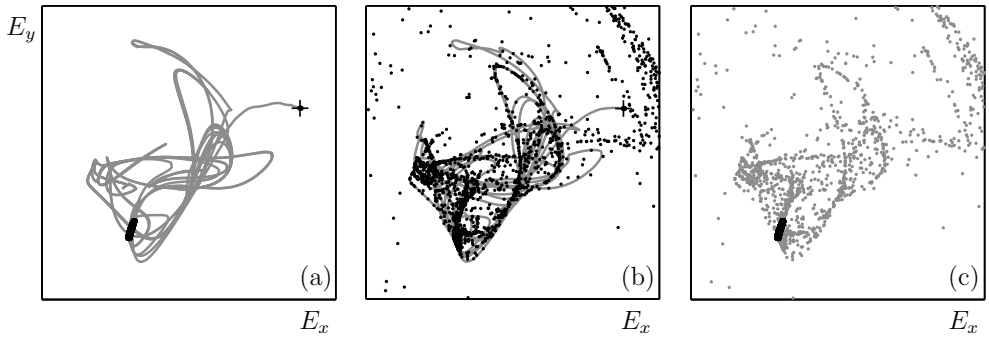

Figure 5.17: Crisis bifurcation responsible for a sudden transition to chaos in the PCF laser (see text for details); the region shown is $E \in [-95, 105] \times [235, 275]$ and $I = 65.1\,\mathrm{mA}$. Reproduced from K. Green and B. Krauskopf, *Physica D*, 173(1-2) (2002) 114–129 ©2002 by Elsevier Science.

to additional damped oscillations as the laser settles down to periodic output. As $\kappa\tau$ is increased further the 1D unstable manifolds make longer and longer excursions before converging to the attractors, becoming increasingly folded and stretched in the process; see panels (d) and (e). This means that there are increasingly complicated transients in the system. Finally, for $\kappa\tau = 2.531$ the 1D unstable manifolds cover a large part of the upper part of the E-plane (f).

At $\kappa\tau \approx 2.570$ there is a sudden transition to chaos with a discontinuous change in the size or shape of the attractor. This is indicative of a crisis bifurcation [22, 23, 51]. At the crisis bifurcation there is a rearrangement of stable and unstable manifolds of suitable saddle points. Figures 5.17 (a) and (b) show for one (of the five) saddle points one branch of the 1D unstable manifold just before and just after the crisis bifurcation. For $\kappa\tau = 2.569$ (a) the branch ends up, after a long transient, at an attracting invariant circle, the intersection of the attracting hose-like torus with Σ. Just after the crisis bifurcation at $\kappa\tau = 2.571$ (b) the 1D unstable manifold accumulates on a large chaotic attractor. Notice that the initial piece of the manifold that was computed does not change much. In Fig. 5.17 (c) the attracting invariant circle that exists before the crisis bifurcation is overlayed (in black) on top of the chaotic attractor (in grey) that exists after the crisis bifurcation. This shows that one is indeed dealing with a crisis bifurcation, in which the small hose-like torus suddenly and discontinuously changes in size to become a much larger chaotic attractor.

5.5 Concluding remarks

Bifurcation analysis is a powerful tool to unravel the dynamics and bifurcations of lasers with delay as modelled by delay differential equations. In particular, transitions to chaos can now be studied in unprecedented detail. This has been demonstrated here with the review of recent work on the COF and PCF lasers. While this work consists largely of theoretical studies of the respective rate equations, there is good reason to believe that bifurcation analysis will be increasingly helpful in the explanation and prediction of experimental results. A first example of a qualitative interpretation of an experiment of a laser with delay (COF in the short cavity regime) can be found in Ref. [34]. It is an important challenge for future work to provide qualitative and quantitative connections between theoretical results on the dynamics of lasers with delay and the physics of actual laser devices in experiments.

This chapter is an attempt to sketch the present state-of-the-art of a young and developing field. Recent results not discussed in detail here can be found in, for example, Refs. [12, 53, 54, 64]. At present more work on the bifurcation analysis of a number of laser systems featuring delay is in progress, including lasers with COF and PCF, and mutually coupled lasers. The list of publications in the field is likely to grow quite rapidly in the coming years.

Honesty demands to mention again that bifurcation theory for DDEs and the associated numerical methods are not straightforward to learn. To help the interested reader, this chapter summarised the relevant theory on DDEs from the point of view of applying it to lasers with delay. Furthermore, the numerical methods were explained in more detail than appears to be necessary to the reader who is mainly interested in the results of their application to laser systems. While it may be useful to skip over the more technical sections in a first reading, this chapter also aims at providing a self-contained review of the underlying theory, that can act as a possible entry point to the even more technical mathematical literature.

Regardless of the background of the reader, the author hopes that this chapter managed to convey the possibilities and the excitement of the bifurcation analysis of lasers with delay!

Acknowledgements

My sincere thanks go to Kirk Green for his input and many valuable suggestions on a draft of this chapter, to Vivi Rottschäfer for collaborating on the computations in Secs. 5.3.2 and 5.3.3, and to Matthias Wolfrum and Bart Haegeman for providing electronic originals of Figs. 5.5 and Figs. 5.6–5.7, respectively. Furthermore I thank my other colleagues with whom I had the pleasure of working on the dynamics and bifurcations of delay lasers over the years. Finally, I gratefully acknowledge the support of my research by an Advanced Research Fellowship grant from the Engineering and Physical Sciences Research Council (EPSRC).

Bibliography

[1] G. P. Agrawal and G. R. Gray, *Effect of phase-conjugate feedback on the noise characteristics of semiconductor lasers*, Phys. Rev. A, 46 (1992), pp. 5890–5898.

[2] P. M. Alsing, V. Kovanis, A. Gavrielides, and T. Erneux, *Lang and Kobayashi phase equation*, Phys. Rev. A, 53 (1996), pp. 4429–4434.

[3] A. R. Champneys, Y. A. Kuznetsov, and B. Sandstede, *A numerical toolbox for homoclinic bifurcation analysis*, Int. J. Bif. Chaos, 6 (1996), pp. 867–887.

[4] D. H. DeTienne, G. R. Gray, G. P. Agrawal, and D. Lenstra, *Semiconductor laser dynamics for feedback from a finite-penetration-depth phase-conjugate mirror*, IEEE J. Quantum Electron., 33 (1997), pp. 838–844.

[5] O. Diekmann, S. A. Van Gils, S. M. Verduyn Lunel, and H. O. Walther, *Delay Equations: Functional-, Complex-, and Nonlinear Analysis*, vol. 110, Springer-Verlag, New York, 1995.

[6] E. Doedel, T. Fairgrieve, B. Sandstede, A. Champneys, Y. Kuznetsov, and X. Wang, *AUTO 97: Continuation and bifurcation software for ordinary differential equations*, 1997. (Software available at `http://indy.cs.concordia.ca/auto/main.html`)

[7] K. Engelborghs, T. Luzyanina, K. in't Hout, and D. Roose, *Collocation methods for the computation of periodic solutions of delay differential equations*, SIAM J. Sci. Comput., 22 (2000), pp. 1593–1609.

[8] K. Engelborghs, T. Luzyanina, and D. Roose, *Numerical bifurcation analysis of delay differential equations using DDE-BIFTOOL*, ACM Transactions Math. Software, 28(1) (2002), pp. 1–21.

[9] K. Engelborghs, T. Luzyanina, and G. Samaey, *DDE-BIFTOOL v2.00: a Matlab package for bifurcation analysis of delay differential equations*, Tech. Rep. TW-330, Department of Computer Science, Katholieke Universiteit Leuven, Belguim, 2000. (Software available at `http://www.cs.kuleuven.ac.be/~koen/delay/ddebiftool.shtml`)

[10] T. Erneux, *Multiple time scale analysis of lasers*, in [40], pp. 54–65.

[11] T. Erneux and A. Gavrielides, *Analytical theory of external cavity modes of a semiconductor laser with phase conjugate feedback*, in M. Osinski, H. Amano, and P. Blood (Eds.), *Physics and Simulation of Optoelectronic Devices XI*, Proceeding of SPIE 4986 (2003), The Society of Photo-Optical Instrumentation Engineers, Bellingham (Washington), to appear.

[12] T. Erneux, A. Gavrielides, and M. Sciamanna, *Stable microwave oscillations due to external-cavity-mode beating in laser diodes subject to optical feedback*, Phys. Rev. A, 66 (2002) 033809.

[13] T. Erneux, F. Rogister, A. Gavrielides, and V. Kovanis, *Bifurcation to mixed external cavity mode solutions for semiconductor lasers subject to optical feedback*, Opt. Commun., 183 (2002), pp. 467–477.

[14] I. Fischer, T. Heil, and W. Elsässer, *Emission dynamics of semiconductor lasers subject to delayed optical feedback*, in [40], pp. 218–237.

[15] I. Fischer, Y. Liu, and P. Davis, *Synchronization of chaotic semiconductor laser dynamics on subnanosecond time scales and its potential for chaos communication*, Phys. Rev. A, 62 (2000) 011801.

[16] A. Gavrielides, *Nonlinear dynamics of semiconductor lasers: Theory and experiments*, in [40], pp. 191–217.

[17] C. R. Giuliano, *Applications of optical phase conjugation*, Physics Today, 34 (1981), pp. 27–35.

[18] P. Glendinning and C. Sparrow, *T-points: A codimension two heteroclinic bifurcation*, Journal of Statist. Phys., 43 (1986), pp. 479–488.

[19] H. Glüsing-Lüerssen, *A behavioural approach to delay-differential systems*, SIAM J. Control Optim., 35(2) (1997), pp. 480–499.

[20] G. R. Gray, D. H. DeTienne, and G. P. Agrawal, *Mode locking in semiconductor lasers by phase-conjugate optical feedback*, Opt. Lett., 20(11) (1995), pp. 1295–1297.

[21] G. R. Gray, D. Huang, and G. P. Agrawal, *Chaotic dynamics of semiconductor lasers with phase-conjugate feedback*, Phys. Rev. A, 49 (1994), pp. 2096–2105.

[22] C. Grebogi, E. Ott, F. Romeiras, and J. A. Yorke, *Critical exponents for crisis-induced intermittency*, Phys. Rev. A, 36(11) (1987), pp. 5365–5380.

[23] C. Grebogi, E. Ott, and J. A. Yorke, *Critical exponent of chaotic transients in nonlinear dynamical systems*, Phys. Rev. Lett., 57(11) (1986), pp. 1284–1287.

[24] K. Green and B. Krauskopf, *Global bifurcations and bistability at the locking boundaries of a semiconductor laser with phase-conjugate feedback* Phys. Rev. E, 66 (2002) 073207.

[25] K. Green and B. Krauskopf, *Bifurcation analysis of frequency locking in a semiconductor laser with phase-conjugate feedback*, Int. J. Bif. Chaos, 13(9) (2003), to appear.

[26] K. Green, B. Krauskopf, and K. Engelborghs, *Bistability and torus break-up in a semiconductor laser with phase-conjugate feedback*, Physica D, 173(1-2) (2002), pp. 114–129.

[27] K. Green, B. Krauskopf, and K. Engelborghs, *One-dimensional unstable eigenfunction and manifold computations in delay differential equations*, Appl. Nonlin. Maths. Research Report 2003.5, University of Bristol 2003. (vailable at `http://www.enm.bris.ac.uk/anm/preprints/2003r05.html`)

[28] K. Green, B. Krauskopf, and G. Samaey, *A two-parameter study of the locking region of a semiconductor laser subject to phase-conjugate feedback*, SIAM J. Appl. Dynam. Syst., 2(2) (2003), pp. 254–276.

[29] J. Guckenheimer and P. Holmes, *Nonlinear Oscillations, Dynamical Systems, and Bifurcations of Vector Fields*, Springer-Verlag, 1993.

[30] B. Haegeman, K. Engelborghs, D. Roose, D. Pieroux, and T. Erneux, *Stability and rupture of bifurcation bridges in semiconductor lasers subject to optical feedback*, Phys. Rev. E, 66 (2002) 046216.

[31] J. K. Hale and S. M. Verduyn Lunel, *Introduction to Functional Differential Equations*, Springer-Verlag, New York, 1993.

[32] T. Heil, I. Fischer, W. Elsässer, and A. Gavrielides, *Dynamics of semiconductor lasers subject to delayed optical feedback: the short cavity regime*, Phys. Rev. Lett., 87 (2001) 243901.

[33] T. Heil, I. Fischer, W. Elsässer, J. Mulet, and C.R.Mirasso, *Chaos synchronization and spontaneous symmetry breaking in symmetrically delay coupled semiconductor lasers*, Phys. Rev. Lett. 86 (2001), pp. 795–798.

[34] T. Heil, I. Fischer, W. Elsässer, B. Krauskopf, K. Green, and A. Gavrielides, *Delay dynamics of semiconductor lasers with short cavities: bifurcations scenarios and mechanisms*, Phys. Rev. E, 67(6) (2003) 066214.

[35] N. Korneyev, M. Radziunas, H.-J. Wünsche, and F. Henneberger, *Bifurcations of a DFB laser with short optical feedback: numerical experiment*, in M. Osinski, H. Amano, and P. Blood (Eds.), *Physics and Simulation of Optoelectronic Devices XI*, Proceeding of SPIE 4986 (2003), The Society of Photo-Optical Instrumentation Engineers, Bellingham (Washington), to appear.

[36] B. Krauskopf, *Bifurcation analysis of laser systems*, in [40], pp. 1–30.

[37] B. Krauskopf, *Strong resonances and Takens's Utrecht Preprint*, in H.W. Broer, B. Krauskopf and G. Vegter (Eds.), *Global Analysis of Dynamical Systems*, Institute of Physics Publishing, Bristol, 2001, pp. 89–111.

[38] B. Krauskopf, G. R. Gray, and D. Lenstra, *Semiconductor laser with phase-conjugate feedback: Dynamics and bifurcations*, Phys. Rev. E, 58 (1998), pp. 7190–7196.

[39] B. Krauskopf and K. Green, *Computing unstable manifolds of periodic orbits in delay differential equations*, J. Comput. Phys., 186(1) (2003), pp. 230–249.

[40] B. Krauskopf and D. Lenstra (Eds.), *Fundamental Issues of Nonlinear Laser Dynamics*, AIP Conference Proceedings 548, American Institute of Physics Publishing, Melville (New York), 2000.

[41] B. Krauskopf and H. M. Osinga, *Growing 1D and quasi-2D unstable manifolds of maps*, J. Comput. Phys., 146 (1998), pp. 404–419.

[42] B. Krauskopf and H. M. Osinga, *Investigating torus bifurcations in the forced Van der Pol oscillator*, in E. J. Doedel and L. S. Tuckerman (Eds.), *Numerical Methods for Bifurcation Problems and Large-Scale Dynamical Systems*, IMA Volumes in Mathematics and its Applications 119, Springer-Verlag, New York, 2000, pp. 199–208.

[43] B. Krauskopf, G. H. M. Van Tartwijk, and G. R. Gray, *Symmetry properties of lasers subject to optical feedback*, Opt. Commun., 177 (2000), pp. 347–353.

[44] Y. Kuznetsov, *Elements of Applied Bifurcation Theory*, Springer-Verlag, New York, 1995.

[45] R. Lang and K. Kobayashi, *External optical feedback effects on semiconductor injection laser properties*, IEEE J. Quantum Electron., QE-16 (1980), pp. 347–355.

[46] T. Luzyanina, K. Engelborghs, and D. Roose, *Numerical bifurcation analysis of differential equations with state-dependent delays*, Int. J. Bif. Chaos, 11 (2001), pp. 737–754.

[47] J. Mørk, B. Tromborg, and J. Mark, *Chaos in semiconductor lasers with optical feedback: Theory and experiment*, IEEE J. Quantum Elec., 28 (1992), pp. 93–107.

[48] J. D. Murray, *Mathematical Biology*, vol. 19, Springer-Verlag, New York, 1980.

[49] D. Pieroux, T. Erneux, B. Haegeman, K. Engelborghs, and D. Roose, *Bridges of periodic solutions and tori in semiconductor lasers subject to delay*, Phys. Rev. Lett., 87 (2001) 193901.

[50] D. Pieroux, T. Erneux, T. Luzyanina, and K. Engelborghs, *Interacting pairs of periodic solutions lead to tori in lasers subject to delayed feedback*, Phys. Rev. E, 63(3) (2001) 036211.

[51] C. Robert, K. T. Alligood, E. Ott, and J. A. Yorke, *Explosions of chaotic sets*, Physica D, 144 (2000), pp. 44–61.

[52] G. Samaey, K. Engelborghs, and D. Roose, *Numerical computation of connecting orbits in delay differential equations*, Numer. Algorithms, 30 (2002), pp. 335–352.

[53] M. Sciamanna, T. Erneux, F. Rogister, O. Deparis, P. Megret, and M. Blondel, *Bifurcation bridges between external-cavity modes lead to polarization self-modulation in vertical-cavity surface-emitting lasers*, Phys. Rev. A, 65 (2002) 041801.

[54] M. Sciamanna, T. Erneux, A. Gavrielides, V. Kovanis, P. Megret, and M. Blondel, *High frequency dynamics in delayed semiconductor laser with short external cavity*, in M. Osinski, H. Amano, and P. Blood (Eds.), *Physics and Simulation of Optoelectronic Devices XI*, Proceeding of SPIE 4986 (2003), The Society of Photo-Optical Instrumentation Engineers, Bellingham (Washington), to appear.

[55] R. Seydel, *Practical bifurcation and stability analysis: from equilbria to chaos*, Interdisciplinary Applied Mathematics Series, Vol. 5, Springer-Verlag, New York, 1994.

[56] J. Sieber, *Numerical bifurcation analysis for multi-section semiconductor lasers*, SIAM J. of Appl. Dyn. Sys., 1(2) (2002), pp. 248–270.

[57] S. H. Strogatz, *Nonlinear Dynamics and Chaos*, Addison-Wesley, Reading (Massachuetts), 1994.

[58] W. A. van der Graaf, L. Pesquera, and D. Lenstra, *Stability and Noise Properties of Diode Lasers with Phase-Conjugate Feedback*, IEEE J. Quantum Electron., 37(4) (2002), pp. 562–573.

[59] G. H. M. Van Tartwijk and G. P. Agrawal, *Laser instabilities: a modern perspective*, Prog. Quantum Electron., 22 (1998), pp. 43–122.

[60] G. H. M. Van Tartwijk and D. Lenstra, *Semiconductor lasers with optical injection and feedback*, Quantum Semiclass. Opt., 7 (1995), pp. 87–143.

[61] G. H. M. Van Tartwijk, H. J. C. Van der Linden, and D. Lenstra, *Theory of a diode laser with phase-conjugate feedback*, Opt. Lett., 17 (1995), pp. 1590–1592.

[62] G. D. Van Wiggeren and R. Roy, *Communication with chaotic lasers*, Science, 279 (1998), pp. 1198–1200.

[63] S. M. Verduyn Lunel and B. Krauskopf, *The mathematics of delay equations with an application to the Lang-Kobayashi equations*, in [40], pp. 66–86.

[64] R. Vincente, J. Mulet, C. R. Mirasso, S. Tang, and J.-M. Liu, *Dynamical properties of two semiconductor lasers with bidirectional optoelectronic coupling*, in M. Osinski, H. Amano, and P. Blood (Eds.), *Physics and Simulation of Optoelectronic Devices XI*, Proceeding of SPIE 4986 (2003), The Society of Photo-Optical Instrumentation Engineers, Bellingham (Washington), to appear.

[65] S. Wieczorek, B. Krauskopf, and D. Lenstra, *A unifying view of bifurcations in a semiconductor laser subject to optical injection*, Opt. Commun., 172 (1999), pp. 279–295.

[66] S. Wieczorek, B. Krauskopf, and D. Lenstra, *Unnested islands of period-doubling in an injected semiconductor laser*, Phys. Rev. E, 84 (2001) 056204.

[67] S. Wieczorek, T. B. Simpson, B. Krauskopf, and D. Lenstra, *Global quantitative predictions of complex laser dynamics*, Phys. Rev. E, 65 (2002) 045207(R)

[68] S. Wieczorek, T. B. Simpson, B. Krauskopf, and D. Lenstra, *Bifurcation transitions in an optically injected diode laser: theory and experiment*, Optics Commun., 215(1-3) (2003), pp. 125–134.

[69] M. Wolfrum and D. Turaev, *Instabilities of lasers with moderately delayed optical feedback*, Opt. Commun., 212 (2002), pp. 127–138.

[70] X. S. Yao and L. Maleki, *Dual microwave and optical oscillator*, Opt. Letters, 22 (1997), pp. 1867–1869.